Inertia-free Attitude Control Laws Based on Rotation Matrices for Spacecraft with Torquers, Thrusters, and Wheels

Avishai Weiss[*], Gerardo Cruz[†], Kshitij Agarwal[‡],
Yousaf Rahman[§], Madhura Medikeri[¶], Antai Xie[||], Marc Camblor[**],
Ilya Kolmanovsky[††] and Dennis S. Bernstein[‡‡]
University of Michigan, Ann Arbor, MI, USA

This paper investigates the performance of three types of fixed-gain and adaptive control laws that require little or no prior modeling of the spacecraft mass distribution. The first type consists of fixed-gain PD/PID control laws; the second type consists of adaptive control laws that involve inertia estimates; and the third type is based on retrospective cost adaptive control. All three methods are based on rotation matrices for representing attitude, which facilitates singularity-free control laws. Furthermore, in the case of Lyapunov-based continuous-time control laws, rotation matrices provide the ability to avoid unwinding without discontinuous switching, which is needed when quaternions are used. We apply these control laws to motion-to-rest and motion-to-spin maneuvers involving rate and/or attitude measurements. Several types of actuators are considered, including magnetic torquers, on-off thrusters, reaction wheels, and single-gimbal control-moment gyros. Simulation results are given to illustrate the robustness of the controllers to uncertainty in the spacecraft inertia. We also investigate closed-loop performance under additional effects, including: actuator misalignment relative to sensor alignment; torque disturbances, such as due to air drag, solar pressure, magnetic torques, and gravity gradients, which are possibly attitude-dependent and which may have unknown spectrum; sensor noise, such as gyro bias and noisy magnetic field measurements; and actuator nonlinearities, such as torque amplitude saturation, on-off torque profile, and unknown deadzone.

---

[*]Graduate Student, Aerospace Engineering Department
[†]Graduate Student, Aerospace Engineering Department
[‡]Graduate Student, Aerospace Engineering Department
[§]Graduate Student, Aerospace Engineering Department
[¶]Graduate Student, Aerospace Engineering Department
[||]Graduate Student, Aerospace Engineering Department
[**]Graduate Student, Aerospace Engineering Department
[††]Professor, Aerospace Engineering Department
[‡‡]Professor, Aerospace Engineering Department

I.   Introduction

Despite the vast range of control laws that have been developed for spacecraft attitude control, the development of an attitude control system remains a labor-intensive, time-consuming process. Among the many reasons for this is the fact that attitude control systems typically depend on a high-fidelity characterization of the spacecraft inertia, including the directions of the principal axes and the principal moments of inertia. To alleviate the need for inertia modeling, this paper focuses on spacecraft attitude control laws that require little or no modeling of the spacecraft's mass distribution. The desire for inertia-free control laws stems from the fact that determining the mass properties of a spacecraft is a tedious and expensive process. Furthermore, fuel usage, shape changes due to on-orbit deployment of structural components, articulated appendages, and docking may change the mass distribution of a spacecraft in ways that are difficult to model.

Inertia-free attitude control laws are available for motion-to-rest maneuvers under various types of actuation. For the case of magnetic torquing, the classical "bdot" control law [1,2] uses rate measurements and measurements of the magnetic field to bring the spacecraft to rest at an unspecified attitude, while the inertia-free control laws given in [3–5] bring the spacecraft to a specified attitude. An adaptive inertia-free attitude control law is given in [6] within the context of achieving minimum-time maneuvers. Inertia-free control laws for motion-to-rest and tracking are given in [7–9].

Attitude control laws can exploit various parameterizations of the rotation group SO(3) [10]. Euler angles are conceptually the simplest representation, but these suffer from the inability to represent all angular velocities at certain 90-degree attitudes; this phenomenon is called gimbal lock since it is reminiscent of the *physical* constraint on the motion of a 3-gimbal mechanism. A related obstacle arises in the use of Rodrigues (Gibbs) parameters and modified Rodrigues parameters, which have singularities at 180 degrees and 360 degrees attitude, respectively [11, pp. 102–111]. The most common attitude representation is based on the Euler parameters (quaternions), which are elements of the four-dimensional unit sphere S^3. The advantage of Euler parameters is the fact that they can represent all attitudes and all angular velocities, with the slight disadvantage that, unlike Euler angles, Rodrigues parameters, and modified Rodrigues parameters, which involve three parameters, Euler parameters involve four parameters that must satisfy a constraint.

A more subtle drawback of Euler parameters, however, is the fact that they provide a double cover of SO(3), that is, each physical attitude is represented by two elements of S^3. This means that the desired attitude has two representations, and thus a controller designed to yield global asymptotic stability on the set of Euler parameters could inadvertently command the spacecraft to needlessly rotate a full 360 degrees. To illustrate these difficulties in a simpler context, we can consider rotation of a rigid body about a fixed axis, that is, motion around a circle. Covering the unit circle with the real line and with the origin 0 viewed as distinct from 2π leads to controllers that rotate the body needlessly from 2π to zero. The difficulty is due to the fact that 0 and 2π represent

distinct values on the real line $\mathbb{R}$ but correspond to the same physical configuration. In three-dimensional rotation, the same phenomenon arises from the fact that S^3 is a double cover of SO(3). This is the unwinding problem, which refers to unnecessary and undesirable rotation away from and back to the desired physical orientation [12]. The inertia-free, quaternion-based control laws in [8, 13, 14] exhibit unwinding.

There are two distinct approaches to avoiding unwinding. The traditional approach is to implement a logic statement that confines the Euler parameters to a unit hemisphere in four-dimensional space, which effectively removes the double covering of the rotation matrices by the Euler parameters. This approach is taken, for example, in [15]. The drawback of this approach, however, is the fact that it introduces a discontinuity and therefore a discontinuous control law, which can lead to chattering in the presence of noise. This issue and associated complications are addressed in [16]. Additional complications relating to discontinuous differential equations are discussed in [17].

An alternative approach to avoiding unwinding is to represent attitude in terms of rotation matrices. Although this approach would seem inefficient due to the need to update 9 parameters satisfying 6 constraints, rotation matrices provide a one-to-one representation of physical attitude without attitude or angular-velocity singularities [18]. Attitude control on SO(3) thus provides the ability to implement continuous control laws that do not exhibit unwinding [19–21]. Inertia-free control laws on SO(3) are developed in [22]. Attitude estimation in terms of rotation matrices is studied in [23–25].

Since SO(3) is a compact manifold, every continuous vector field on it necessarily possesses more than one equilibrium, in fact, at least four. This means that global convergence on SO(3) under continuous time-invariant control is impossible. Consequently, the objective of [20–22] is almost global stabilization, where the spurious equilibria are saddle points. Although the spurious equilibria can slow the rate of convergence for certain initial conditions, this approach provides an alternative to the complications of discontinuous control laws.

II. Objectives of this Study

As outlined above, this paper focuses on the control of rigid spacecraft using inertia-free control laws based on rotation matrices. The control laws that we consider are of three types. The first type comprises *fixed-gain attitude control laws* (FGAC). These control laws take the form of PD/PID control laws tailored to the nonlinear characteristics of spacecraft dynamics. Since linearized rigid-body dynamics comprise a double integrator about each principal axis, we expect that asymptotic tracking of attitude ramp commands (that is, spin maneuvers) about each principal axis is possible without integral action. Therefore, the primary role of integral control is to reject constant disturbances. In the simplest case of PD control only, an FGAC controller that uses rotation matrices is given in [26]. We also consider an extension of the PD control law that includes integral action. We refer to these control laws as SO(3)/0 and SO(3)/3, respectively. FGAC extensions to reaction wheels and control moment gyros (CMG's) are presented in [27, 28].

The second type of controller is an extension of fixed-gain attitude control laws to include an on-line estimate of the spacecraft inertia. This type of control law, called *estimation-based attitude control* (EBAC), is considered in [8] using quaternions and in [22] using rotation matrices. The control law given in [22] includes 9 integrators, three of which are in the feedback path and 6 of which arise from the inertia estimate but are not in the feedback path. We also consider a simplification of this control law that involves only the integrators arising from the inertia estimate. We refer to these control laws as SO(3)/9 and SO(3)/6, respectively. The EBAC controller given in [22] applies to thrusters without saturation; extensions to address saturation are given in [29]. The EBAC controller is developed for reaction wheels in [27]. Extensions to the case of fixed-speed, single-gimbal CMG's with velocity-commanded gimbals is considered in [28]. This approach provides direct control of the gimbal rates without an intermediary steering law as in [30].

The third type of controller is *retrospective cost attitude control* (RCAC), which is based on a retrospective cost criterion for updating the controller. Retrospective cost adaptive control is developed for linear systems in [31–36] for stabilization, command following, disturbance rejection, and model reference control. This approach has been employed in [37,38] to investigate the ability of RCAC to control systems with unmodeled nonlinearities. We take a similar approach in the present paper by applying RCAC to spacecraft attitude control. Our results are based on the application of RCAC to attitude control involving thrusters in [39] and reaction wheels in [40].

For each control law we consider various types of torque actuation. These include magnetic torquers, thrusters, reaction wheels, and single-gimbal CMG's. Magnetic torquers require electrical energy, which is renewable, and provide low levels of torque to modify the angular momentum of the spacecraft. Thrusters can also modify the angular momentum of the spacecraft, but require a source of consumable on-board fuel, which limits the life of the spacecraft. Like magnetic torquers, reaction wheels and CMG's require only electrical energy, but are not able to modify the total angular momentum of the spacecraft-plus-wheels. Consequently, the cumulative effect of torque disturbances causes reaction wheels and CMG's to spin up, and these devices must subsequently be de-saturated by magnetic torquers and/or thrusters.

We assume that for thrusters and wheels the spacecraft is fully actuated in the sense that the actuators can provide torque about three independent spacecraft axes. However, the torque produced on the spacecraft by magnetic torquers lies in the plane that is perpendicular to the local direction of Earth's geomagnetic field. The spacecraft is thus, at each time instant, underactuated. Nevertheless, Earth's geomagnetic field is sufficiently varying in time and space that, for orbits not coinciding with Earth's magnetic equator (when using a nonrotating dipole model of the geomagnetic field), the spacecraft is controllable [41].

Since the spacecraft inertia is unknown, we do not assume that we know the directions of the principal axes of inertia. However, we assume that a body-fixed frame is specified and that the alignment of the sensors and actuators is also specified relative to that frame. We view the attitude sensor (for example, a star tracker) as the truth

sensor, and thus its alignment relative to the body frame is assumed to be exact and known. The alignment of the gyros and actuators relative to the body-fixed frame is also assumed to be exact and known except where noted.

To illustrate various control laws, we consider two basic scenarios, namely, motion-to-rest (M2R) maneuvers and motion-to-spin (M2S) maneuvers, where "rest" and "spin" refer to motion relative to an inertial frame. An M2R maneuver may begin from either rest or an arbitrary angular velocity. Hence, M2R includes maneuvers commonly referred to as slews, detumbling, and stabilization. The goal is to have the spacecraft come to rest with a specified attitude in the sense that a specified body axis is pointing in a specified inertial direction. If the M2R and M2S maneuvers begin from zero angular velocity, then we use the terminology rest-to-rest (R2R) and rest-to-spin (R2S), respectively. In some cases we consider the more limited objective of bringing the spacecraft to rest without specifying an inertial direction.

An M2S maneuver aims to bring the spacecraft from an arbitrary initial angular velocity and attitude to a constant angular velocity relative to an inertial frame. Consequently, the goal is to have the spacecraft rotate at a constant rate about a body-fixed axis whose inertial direction is fixed. Specified spin maneuvers can be used, for example, to provide momentum bias to the spacecraft, or to achieve nadir pointing along a circular orbit. Although the spacecraft inertia is unknown, and thus the directions of the principal axes of inertia are unknown, we consider commanded spins about both principal and non-principal axes in order to demonstrate how these control laws perform in this situation. A commanded spin about a principal axis has the advantage that, once the spacecraft reaches the desired spin, no additional torque is needed in the absence of disturbances except possibly to maintain a spin about the minimum and intermediate axes, where the latter is naturally unstable and the former is unstable due to energy dissipation. Of course, a commanded spin about a non-principal axis requires constant, nonzero torques, and thus is more sensitive to torque saturation.

For each of these scenarios, we consider various effects that can degrade the performance of the controller, with the goal of assessing the ability of the control laws to deal with effects that are not explicitly addressed by the control laws. For example, during M2R and M2S maneuvers, the spacecraft may be subjected to torque disturbances. These disturbances may be due to atmospheric drag, solar pressure, magnetic torques, gravity gradients, and on-board devices, and thus they may depend on the attitude of the spacecraft as well as its location along its orbit. The disturbances may be constant, sinusoidal, or random, with possibly unknown spectrum.

The sensors used for attitude control may be corrupted by noise. We view the attitude sensor as the truth sensor, and thus the control system attempts to have the measured attitude follow the attitude command. The gyro measurements, however, may be corrupted by bias (drift), sinusoidal, or random noise with unknown spectrum. In addition, the gyros may be misaligned in an unknown way relative to the attitude sensor. Likewise, the actuators may be misaligned relative to the attitude sensor.

Finally, the operation of the actuators may be affected by nonlinearities. For exam-

ple, all real actuators are subject to magnitude saturation, whose range is usually known. In addition, an unknown deadzone nonlinearity may be present in the actuators, while a known deadzone nonlinearity may be intentionally introduced to limit fuel consumption for stationkeeping. Finally, thrusters are usually operated in an on-off mode, which constitutes a nonlinearity whose characteristics are usually known.

III.   Spacecraft Model, Assumptions, and Control Objectives

As a spacecraft model, we consider a single rigid spacecraft bus controlled by magnetic torquers, thrusters, reaction wheels, or single-gimbal CMG's. The spacecraft's angular momentum H, relative to its center of mass with respect to the inertial frame resolved in the spacecraft frame, depends on the type of torque actuation used and is detailed below for the aforementioned cases. We consider only the rotational motion of the spacecraft and not the translational motion of the spacecraft's center of mass; therefore we consider only the torque τ_{actuator} applied by the force or torque actuators. We assume that a body-fixed frame is defined for the spacecraft, whose origin is chosen to be the center of mass, and that an inertial frame is specified for determining the attitude of the spacecraft. The spacecraft equations of motion are given by Euler's equation and Poisson's equation

$$J\dot{\omega} = H \times \omega + \tau_{\text{actuator}} + z_{\text{dist}}, \tag{1}$$

$$\dot{R} = R\omega^{\times}, \tag{2}$$

where $\omega \in \mathbb{R}^3$ is the angular velocity of the spacecraft frame with respect to the inertial frame resolved in the spacecraft frame, $\omega^{\times}$ is the cross-product matrix of ω, $J \in \mathbb{R}^{3\times3}$ is the constant, positive-definite inertia matrix of the spacecraft including wheels if present, that is, the inertia tensor of the spacecraft relative to the spacecraft center of mass resolved in the spacecraft frame, and $R = \mathcal{O}_{\text{In/SC}} \in \mathbb{R}^{3\times3}$ is the rotation tensor that transforms the inertial frame into the spacecraft frame resolved in the spacecraft frame, and where $\mathcal{O}_{\text{In/SC}}$ is the orientation (direction cosine) matrix that transforms components of a vector resolved in spacecraft frame into the components of the same vector resolved in inertial frame.

The components of the vector τ_{actuator} represent the torque inputs about each axis of the spacecraft frame, which depends on the chosen torque actuation as detailed below. The vector z_{dist} represents disturbance torques, that is, all internal and external torques applied to the spacecraft aside from control torques, which may be due to onboard components, gravity gradients, solar pressure, atmospheric drag, or the ambient magnetic field. For convenience in (1), (2) we omit the argument t, recognizing that ω, R, u, and z_{dist} are time-varying quantities.

A. Measurement Sensors

Both rate (inertial) and attitude (noninertial) measurements are assumed to be available. Gyro measurements $y_{\text{rate}} \in \mathbb{R}^3$ are assumed to provide measurements of the angular velocity resolved in the spacecraft frame, that is,

$$y_{\text{rate}} = \omega. \tag{3}$$

For simplicity, we assume that gyro measurements are available without noise and without bias. In practice, bias can be corrected by using attitude measurements.

Attitude is measured indirectly through direction measurements using sensors such as star trackers and represented as the output

$$y_{\text{attitude}} = R. \tag{4}$$

When attitude measurements are given in terms of an alternative attitude representation, such as quaternions, Rodrigues's formula can be used to determine the corresponding rotation matrix. Attitude estimation on SO(3) is considered in [23–25].

The objective of the attitude control problem is to determine control inputs such that the spacecraft attitude given by R follows a commanded attitude trajectory given by the possibly time-varying C^1 rotation matrix $R_{\text{d}}(t)$. For $t \geq 0$, $R_{\text{d}}(t)$ is given by

$$\dot{R}_{\text{d}}(t) = R_{\text{d}}(t)\omega_{\text{d}}(t)^\times, \tag{5}$$
$$R_{\text{d}}(0) = R_{\text{d}0}, \tag{6}$$

where ω_{d} is the desired possibly time-varying angular velocity. The error between $R(t)$ and $R_{\text{d}}(t)$ is given in terms of the attitude-error rotation matrix

$$\tilde{R} \overset{\triangle}{=} R_{\text{d}}^{\text{T}} R, \tag{7}$$

which satisfies the differential equation

$$\dot{\tilde{R}} = \tilde{R}\tilde{\omega}^\times, \tag{8}$$

where the angular-velocity error $\tilde{\omega}$ is defined by

$$\tilde{\omega} \overset{\triangle}{=} \omega - \tilde{R}^{\text{T}}\omega_{\text{d}}.$$

B. Attitude Error

A scalar measure of attitude error is given by the rotation angle $e(t)$ about the eigenaxis needed to rotate the spacecraft from its attitude $R(t)$ to the desired attitude

$R_{\mathrm{d}}(t)$. This angle, called the eigenaxis attitude error, is given by

$$e(t) = \cos^{-1}(\tfrac{1}{2}[\operatorname{tr} \tilde{R}(t) - 1]). \tag{9}$$

C. Spacecraft Inertia

Since the control laws in this paper require little or no inertia modeling, we consider examples that span the range of possible inertia matrices for rigid bodies. We view the inertia of a rigid body as determined by its principal moments of inertia, that is, the diagonal entries of the inertia tensor resolved in a principal body-fixed frame, in which case the inertia matrix is a diagonal matrix. If the inertia tensor is resolved in a non-principal body-fixed frame, then the diagonal entries are the moments of inertia and the off-diagonal entries are the products of inertia. The off-diagonal entries of the inertia matrix are thus a consequence of an unknown rotation between a principal body-fixed frame and the chosen body-fixed frame.

Figure 1 shows the triangular region of feasible principal moments of inertia of a rigid body. There are five cases that are highlighted for the principal moments of inertia $\lambda_1 \geq \lambda_2 \geq \lambda_3 > 0$, where $\lambda_1, \lambda_2, \lambda_3$ satisfy the triangle inequality $\lambda_1 < \lambda_2 + \lambda_3$. Let m denote the mass of the rigid body. The point $\lambda_1 = \lambda_2 = \lambda_3$ corresponds to a sphere of radius $R = \sqrt{\frac{5\lambda_1}{2m}}$, a cube whose sides have length $L = \sqrt{\frac{6\lambda_1}{m}}$, and a cylinder of length L and radius R, where $L/R = \sqrt{3}$ and $R = \sqrt{\frac{2\lambda_1}{m}}$. The point $\lambda_1 = \lambda_2 = 2\lambda_3$ corresponds to a cylinder of length L and radius R, where $L/R = 3$ and $R = \sqrt{\frac{2\lambda_1}{m}}$. The point $\lambda_1 = \frac{6}{5}\lambda_2 = 2\lambda_3$, located at the centroid of the triangular region, corresponds to a solid rectangular body with sides $L_1 = \sqrt{\frac{8\lambda_1}{m}} > L_2 = \sqrt{\frac{4\lambda_1}{m}} > L_3 = \sqrt{\frac{2\lambda_1}{m}}$.

The remaining cases in Figure 1 are nonphysical, limiting cases. The point $\lambda_1 = 2\lambda_2 = 2\lambda_3$ corresponds to a thin disk of radius $R = \sqrt{\frac{2\lambda_1}{m}}$. The point $\lambda_1 = \lambda_2$ and $\lambda_3 = 0$ corresponds to a thin cylinder of radius $R = 0$ and length $L = \sqrt{\frac{12\lambda_1}{m}}$. Finally, points along the line segment $\lambda_1 = \lambda_2 + \lambda_3$, where $\lambda_2 > \lambda_3$ correspond to thin rectangular plate with sides of length $L_1 = \sqrt{\frac{12\lambda_2}{m}} > L_2 = \sqrt{\frac{12\lambda_3}{m}}$.

For all simulations of the inertia-free control laws, we view the principal axes as the nominal body-fixed axes, and thus the nominal inertia matrix is a diagonal matrix whose diagonal entries are the principal moments of inertia. Then, to demonstrate robustness, we vary the principal moments as well as the orientation of the body-fixed frame relative to the principal axes. For convenience, we normalize $\lambda_1 = 10$ kg-m^2, and we choose the inertia matrices J_1, J_2, J_3, J_4, J_5 to correspond to the points noted in Figure 1. These matrices, which correspond to the sphere, cylinder with $L/R = 3$, centroid, thin disk,

and thin cylinder, respectively, are defined as

$$J_1 = \text{diag}(10, 10, 10), \quad J_2 = \text{diag}(10, 10, 5), \quad J_3 = \text{diag}(10, 25/3, 5),$$
$$J_4 = \text{diag}(10, 5, 5), \quad J_5 = \text{diag}(10, 10, 0.1). \tag{10}$$

The inertia matrix J_3 corresponding to the centroid of the inertia region serves as the nominal inertia matrix, while the inertia matrices J_1, J_2, J_4, J_5 are used as perturbations to demonstrate robustness of the control laws. A perturbation $J(\alpha)$ of J_i in the direction of J_j thus has the form

$$J(\alpha) = (1 - \alpha)J_i + \alpha J_j, \tag{11}$$

where $\alpha \in [0, 1]$. Finally, in order to facilitate numerical integration of Euler's equation, note that J_5 is chosen to be a nonsingular approximation of the limiting inertia of a thin cylinder.
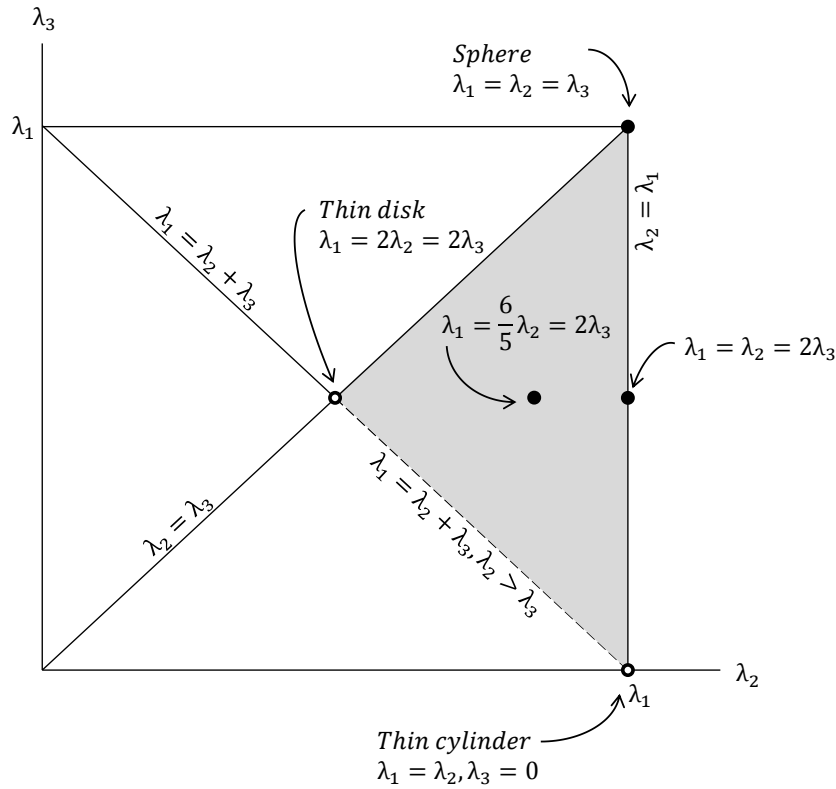
Figure 1. Feasible region of the principal moments of inertia $\lambda_1, \lambda_2, \lambda_3$ of a rigid body satisfying $0 < \lambda_3 \leq \lambda_2 \leq \lambda_1$, where $\lambda_1 < \lambda_2 + \lambda_3$. The shaded region shows all feasible values of λ_2 and λ_3 in terms of the largest principal moment of inertia λ_1. The open dots and dashed line segment indicate nonphysical, limiting cases.

D. Thrusters

For a rigid spacecraft actuated by three independent thrusters, the angular momentum has the form $H = J\omega$, while the actuator torque $\tau_{\text{actuator}} = \tau_{\text{thruster}}$ is due to the thrusters. Therefore, in this case (1) becomes

$$J\dot{\omega} = (J\omega) \times \omega + \tau_{\text{thruster}} + z_{\text{dist}}. \tag{12}$$

Furthermore, the torque due to the thrusters has the form Bu, where the components of the vector $u \in \mathbb{R}^3$ represent three independent torque inputs, and the matrix $B \in \mathbb{R}^{3\times3}$ determines the applied torque about each axis of the spacecraft frame due to u. Therefore, in this case (12) becomes

$$J\dot{\omega} = (J\omega) \times \omega + Bu + z_{\text{dist}}. \tag{13}$$

Thrusters may operate in continuous or on-off mode. In the latter case, the on-off nonlinearity must be considered separately. In addition, it may be desirable to introduce a deadzone nonlinearity and possibly hysteresis logic to avoid chattering and save fuel during stationkeeping.

E. Magnetic Torquers

For a rigid spacecraft actuated by three magnetic torque devices, and without on-board momentum storage, it follows that $H = J\omega$, which, when substituted into (1), yields the equations of motion for a spacecraft with magnetic torquers. For the case of M2R, these equations have the form

$$J\dot{\omega} = (J\omega) \times \omega + \tau_{\text{mag}} + z_{\text{dist}}, \tag{14}$$

where the vector $\tau_{\text{mag}} \in \mathbb{R}^3$ represents the torque on the spacecraft generated by the magnetic actuators. The vector can be written as [42]

$$\tau_{\text{mag}}(t) = u(t) \times b(t) = -b(t)^\times u(t), \tag{15}$$

where $u(t)$ is the magnetic dipole moment generated by the currents in the magnetic actuators measured in ampere-square meters (A-m^2), and where $b(t) = [b_x(t) \quad b_y(t) \quad b_z(t)]^{\text{T}}$ is Earth's geomagnetic field measured in teslas (T) and resolved in the body-fixed frame. For a discussion on generating magnetic dipole moments from magnetic torquer rods, see [43]. Defining

$$B(t) \overset{\triangle}{=} -b(t)^\times, \tag{16}$$

we can rewrite (14) as,

$$J\dot{\omega} = (J\omega) \times \omega + Bu + z_{\text{dist}}. \tag{17}$$

Note that we have dropped the argument t for convenience.

F.   Reaction Wheels

Consider a spacecraft actuated by three axisymmetric wheels attached to a rigid bus in a known and linearly independent, but not necessarily orthogonal, configuration with an arbitrary and unknown orientation relative to the spacecraft principal axes. Each wheel is mounted so that it rotates about one of its own principal axes passing through its own center of mass. However, we do not assume that each wheel's axis of rotation passes through the center of mass of the bus, nor do we assume that the wheels are balanced with respect to the bus in order to preserve the location of the center of mass of the bus. Thus the center of mass of the spacecraft and the center of mass of the bus may be distinct points.

Let the spacecraft be denoted by SC, and let C denote its center of mass. Although the spacecraft is not a rigid body, the axial symmetry of the wheels implies that C is fixed in both the bus and the spacecraft. Assume a bus-fixed frame F_B, three wheel-fixed frames F_{W_i}, whose x-axes are aligned with the rotation axes of their respective wheels, and an Earth-centered inertial frame F_E. Furthermore, let J_{SC} denote the inertia matrix of the spacecraft (that is, bus J_b plus wheels J_w) relative to the spacecraft's center of mass resolved in F_B, and let J_α denote the inertia matrix of the wheel assembly resolved in F_B. The angular momentum of the spacecraft relative to its center of mass with respect to the inertial frame is given by

$$H = J_{SC}\omega + J_\alpha\nu. \tag{18}$$

Therefore, (1) has the form

$$J_{SC}\dot{\omega} = (J_{SC}\omega + J_\alpha\nu) \times \omega + \tau_{RW} + z_{dist}, \tag{19}$$

$$\dot{\nu}_i = \mathcal{O}_{B/W_i}e_1 u_i, \quad i = 1, 2, 3, \tag{20}$$

where

$$J_\alpha \triangleq \left[\begin{array}{ccc} \alpha_1 \mathcal{O}_{B/W_1} e_1 & \alpha_2 \mathcal{O}_{B/W_2} e_1 & \alpha_3 \mathcal{O}_{B/W_3} e_1 \end{array} \right],$$

$$u \triangleq \left[\begin{array}{c} u_1 \\ u_2 \\ u_3 \end{array} \right], \quad \nu \triangleq \left[\begin{array}{c} \nu_1 \\ \nu_2 \\ \nu_3 \end{array} \right] \triangleq \left[\begin{array}{c} \int_0^t u_1(s)\,\mathrm{d}s \\ \int_0^t u_2(s)\,\mathrm{d}s \\ \int_0^t u_3(s)\,\mathrm{d}s \end{array} \right],$$

the components u_1, u_2, u_3 of u are the angular accelerations of the wheels relative to the spacecraft frame with respect to an inertial frame, and $e_1 = [1\ 0\ 0]^T$.

The reaction-wheel torque has the form

$$\tau_{RW} = -J_\alpha u. \tag{21}$$

Therefore, defining

$$B \overset{\triangle}{=} -J_\alpha, \tag{22}$$

the equations of motion for a spacecraft with reaction wheels have the form

$$J_{\text{sc}}\dot{\omega} = (J_{\text{sc}}\omega + J_\alpha \nu) \times \omega + Bu + z_{\text{dist}}, \tag{23}$$

$$\dot{\nu}_i = \mathcal{O}_{\text{B/W}_i} e_1 u_i, \quad i = 1, 2, 3. \tag{24}$$

Note that (24) is a kinematic relation describing the angular acceleration of wheel i. In practice, a servo loop is closed around each reaction wheel in order to produce the desired angular acceleration.

G. CMG's

Consider a spacecraft actuated by three orthogonal single-gimbal CMG's with spherical gyro wheels attached to a rigid bus. Each CMG is mounted so that its gimbal is free to rotate about an axis passing through the center of mass of the gyro wheel. For simplicity, the gimbals are assumed to be massless. However, we do not assume that each gimbal's axis of rotation passes through the center of mass of the bus, nor do we assume that the CMG's are balanced with respect to the bus in order to preserve the location of its center of mass. Thus the center of mass of the spacecraft and the center of mass of the bus may be distinct points.

Let the spacecraft be denoted by SC", and let C denote its center of mass. Although the spacecraft is not a rigid body, the spherical symmetry of the gyro wheels implies that C is fixed in both the bus and the spacecraft. Let c_i denote the center of mass of the ith gyro wheel. We assume a bus-fixed frame F_B, three gimbal-fixed frames F_{G_i} whose y-axes are aligned with the rotation axes of their respective gimbals, three gyro-wheel-fixed frames F_{W_i} whose x-axes are aligned with the rotation axes of their respective gyro wheels, and an Earth-centered inertial frame F_E. The angular momentum of the spacecraft relative to its center of mass with respect to the inertial frame is given by

$$H = J_{\text{SC}}\omega + \sum_{i=1}^{3} \beta_i \omega_{\text{W}_i}. \tag{25}$$

In this case (1) becomes

$$J_{\text{SC}}\dot{\omega} = \left(J_{\text{SC}}\omega + \sum_{i=1}^{3} \beta_i \omega_{\text{W}_i}\right) \times \omega - J_\beta \dot{u} + \tau_{\text{CMG}} + z_{\text{dist}}, \tag{26}$$

where

$$J_\beta \triangleq \begin{bmatrix} \beta_1 & 0 & 0 \\ 0 & \beta_2 & 0 \\ 0 & 0 & \beta_3 \end{bmatrix}, \qquad u \triangleq \begin{bmatrix} u_1 \\ u_2 \\ u_3 \end{bmatrix},$$

and the scalar control u_i is the angular velocity of the ith gimbal. Furthermore, the CMG actuator torque τ_{CMG} has the form

$$\tau_{\text{CMG}} = Bu, \tag{27}$$

where

$$B \triangleq \begin{bmatrix} \beta_1 \left(\omega_{\text{W}_1}^\times - \omega^\times \right) e_1 & \beta_2 \left(\omega_{\text{W}_2}^\times - \omega^\times \right) e_2 & \beta_3 \left(\omega_{\text{W}_3}^\times - \omega^\times \right) e_3 \end{bmatrix}. \tag{28}$$

Note that the actuator matrix B given by (28) is state-dependent and thus time-varying.

Substituting (27) and (28) into (26) yields Euler's equation for a spacecraft with CMG's given by

$$J_{\text{SC}}\dot{\omega} = \left(J_{\text{SC}}\omega + \sum_{i=1}^{3} \beta_i \omega_{\text{W}_i} \right) \times \omega + Bu + z'_{\text{dist}}, \tag{29}$$

where

$$z'_{\text{dist}} \triangleq z_{\text{dist}} - J_\beta \dot{u}. \tag{30}$$

Note that we consider $\dot{u}$ as a component of the disturbance.

IV.   Fixed-Gain Attitude Control (FGAC)

In this section we describe the FGAC control laws for each type of actuation. These control laws involve gains that are, in most cases, constant, and must be chosen by the user based on considerations of control authority and desired closed-loop response. Although the response of the spacecraft depends on the actual inertia of the spacecraft, convergence properties are guaranteed regardless of the spacecraft inertia, which need not be known.

A.   FGAC for Thrusters

The following preliminary results concerning rotation matrices are needed. Let I denote the 3×3 identity matrix, and let M_{ij} denote the i, j entry of the matrix M. The following result provides some properties of a function of rotation matrices that is used to construct a Lyapunov function.

Lemma 1. [22] Let $A \in \mathbb{R}^{3 \times 3}$ be a diagonal positive-definite matrix and let R be a rotation matrix. Then the following statements hold:

i) For all $i, j = 1, 2, 3$, $R_{ij} \in [-1, 1]$.

ii) $\operatorname{tr}(A - AR) \geq 0$.

iii) $\operatorname{tr}(A - AR) = 0$ if and only if $R = I$.

An inertia-free control law for a rigid spacecraft with three torque inputs is given by the proportional-derivative-(PD)-type SO(3)/0 control law [22, 26]

$$u = -B^{-1}(K_{\mathrm{p}} S + K_{\mathrm{v}} \omega), \tag{31}$$

where B is the torque-input matrix, and K_{p} and K_{v} are proportional (attitude) and derivative (angular velocity) gains, respectively. The attitude error S is defined by

$$S \triangleq \sum_{i=1}^{3} a_i (\tilde{R}^{\mathrm{T}} e_i) \times e_i, \tag{32}$$

where a_1, a_2, a_3 are distinct positive numbers such that $A = \operatorname{diag}(a_1, a_2, a_3)$, e_1, e_2, e_3 are the standard basis vectors, and the rotation matrix $\tilde{R} = R R_{\mathrm{d}}^{\mathrm{T}}$ represents the pointing error between the current attitude R and the desired attitude R_{d}. The effect of this controller on the attitude of a rigid spacecraft follows from the Lyapunov function

$$V(\omega, \tilde{R}) \triangleq \tfrac{1}{2} \omega^{\mathrm{T}} J \omega + K_{\mathrm{p}} \operatorname{tr}(A - A\tilde{R}). \tag{33}$$

with its time-derivative along the trajectories of the closed-loop system satisfying

$$\dot{V}(\omega, \tilde{R}) = -\omega^{\mathrm{T}} K_{\mathrm{v}} \omega. \tag{34}$$

This controller is inertia-free since knowledge of the spacecraft inertia J is not needed for implementation. Consequently, this controller can be implemented for stabilization and slew maneuvers without knowledge of the spacecraft's mass distribution.

The controller (31) is amenable to direct enforcement of saturation bounds. The following result is given in [22]. Extensions are given in [29].

Proposition 1. Let α and β be positive numbers, let $A = \operatorname{diag}(a_1, a_2, a_3)$ be a diagonal positive-definite matrix with distinct diagonal entries, and let K_{p} and $K_{\mathrm{v}} = K_{\mathrm{v}}(\omega)$ be given by

$$K_{\mathrm{p}} = \frac{\alpha}{\operatorname{tr} A} \tag{35}$$

and

$$K_{\mathrm{v}} = \beta \begin{bmatrix} \frac{1}{1+|\omega_1|} & 0 & 0 \\ 0 & \frac{1}{1+|\omega_2|} & 0 \\ 0 & 0 & \frac{1}{1+|\omega_3|} \end{bmatrix}. \tag{36}$$

Then, for all $t \geq 0$, the control torque given by (31) satisfies

$$\|u(t)\|_\infty \leq \frac{\alpha + \beta}{\sigma_{\min}(B)}, \tag{37}$$

where $\sigma_{\min}(B)$ denotes the minimum singular value of B.

To include integral action we extend (31) to obtain the SO(3)/3 control law

$$u = -B^{-1}[K_{\mathrm{p}}S + K_{\mathrm{v}}K_1 S + K_{\mathrm{i}}C_{\mathrm{d}}D^{-1}C_{\mathrm{d}}^T \int_0^t (\tilde{\omega}(s) + K_1 S(s))\,\mathrm{d}s + K_{\mathrm{v}}\tilde{\omega}]. \tag{38}$$

This control law is suggested by the EBAC control law (68) given below, by specializing $u = B^{-1}(v_2 + v_3)$. Although SO(3)/3 does not have a known Lyapunov function that ensures closed-loop stability, simulation results suggest that it is stabilizing for all choices of gains K_{p}, K_{v}, and K_{i}.

B.   FGAC for Magnetic Torquers

A challenge in magnetic actuation is the fact that the magnitude and direction of the local geomagnetic field may be uncertain. Although geomagnetic field models are available and are updated periodically [44], these models have limited accuracy, and forecasts of the geomagnetic field may be erroneous due to unmodeled effects and unpredictable disturbances [45]. Consequently, it is desirable to develop control techniques for magnetic actuation that rely solely on current, on-board measurements of the geomagnetic field [46].

For magnetic torquing, a quaternion-based FGAC control law that relies solely on current, on-board measurements of the geomagnetic field and requires knowledge of the spacecraft inertia matrix is given by (13) of [4]. The proof of stability is based on averaging theory. We modify this control law to use rotation matrices rather than quaternions and, inspired by [47], to be inertia free. The proportional-derivative-(PD)-type SO(3)/0 control law is thus given by

$$u = -\frac{b^\times(t)}{\|b(t)\|^2}\bar{\Gamma}^{-1}(\varepsilon^2 K_{\mathrm{p}}S + \varepsilon K_{\mathrm{v}}\omega), \tag{39}$$

where

$$\bar{\Gamma} \triangleq \lim_{T \to \infty} \int_0^T \Gamma(t) \mathrm{d}t = \lim_{T \to \infty} \int_0^T -\frac{b^\times(t) b^\times(t)}{||b(t)||^2},$$

and $0 < \varepsilon < \varepsilon^*$ is a scaling of the proportional and derivative gains K_p and K_v, where ε^* is the maximum scaling. As mentioned in [4], this condition guarantees that the control action changes on the order of the natural time variation of Earth's magnetic field.

C.   FGAC for Reaction Wheels

For the following development we assume that J_α is constant, nonsingular, and known. That is, the spacecraft has three linearly independent, axisymmetric wheels, with known moments of inertia about their spin axes in a known configuration relative to the bus. However, J_sc is assumed to be unknown.

The inertia-free control law for reaction-wheel actuation is given by the proportional-derivative-(PD)-type SO(3)/0 control law [27]

$$u = J_\alpha^{-1}(K_\mathrm{p}S + K_\mathrm{v}\omega). \tag{40}$$

Note that $-J_\alpha$ is substituted for the input matrix B used in (31), but otherwise the controller requires no modification for the case of reaction-wheel actuation. The Lyapunov function

$$V(\omega, \tilde{R}) \triangleq \tfrac{1}{2}\omega^T J_\mathrm{sc}\omega + K_\mathrm{p}\mathrm{tr}(A - A\tilde{R}) \tag{41}$$

and its derivative

$$\dot{V}(\omega, \tilde{R}) = -\omega^T K_\mathrm{v}\omega \tag{42}$$

remain unchanged. Since this control law does not regulate the speed of the wheels, the function V is not a positive-definite function of the angular velocities of the wheels relative to the bus.

D.   FGAC for CMG's

For the following development we assume that J_β is constant, nonsingular, and known. That is, the spacecraft has three orthogonal CMG's with spherical gyro wheels with known moments of inertia about their spin axes.

In addition, we assume that the gimbal accelerations $\dot{u}$ are negligible. We thus ignore the effect of $\dot{u}$ in the derivation of the control law by considering it a part of the disturbance z_d. This treatment of $\dot{u}$ is consistent with [48–50]. We do, however, include this effect in simulations and show through numerical examples that this is a reasonable assumption.

A difficulty encountered with CMG's is that the torque they can generate may be

confined to a plane perpendicular to the requested torque. When this condition occurs, the CMG's are considered to be in a singular state, and gimbal angular velocities that synthesize the requested torque do not exist. Much of the work on CMG's has thus focused on the development of steering laws that modify the requested torque to either avoid these singular states or steer the controller through them [51–55].

While we do not use an explicit steering law to synthesize the desired torque, the matrix B in the CMG case is state-dependent and sometimes singular. Borrowing ideas from the steering-law literature, in the subsequent examples we employ practical, albeit approximate, methods for inverting B. For example, the singularity-robust (SR) inverse [56,57] trades off between introducing torque errors in the vicinity of a singularity and the feasibility of the solution, where feasibility indicates that the gimbal angular velocities remain bounded, unlike the case of the Moore-Penrose inverse.

The SR inverse is derived from the optimization problem

$$\text{minimize} \quad e^{\mathrm{T}}We, \tag{43}$$

where $e = [\tau - Yu \ \ u]^{\mathrm{T}}$, τ is the desired torque in a steering-law formulation of the CMG problem, and $W = \mathrm{diag}(W_1, W_2)$ is a block-diagonal weight matrix.

The SR inverse is thus given by

$$Y^{\#} = W_2^{-1}Y^{\mathrm{T}}\left(YW_2Y^{\mathrm{T}} + W_1^{-1}\right). \tag{44}$$

Note that different values of W_1 and W_2 yield different SR inverses, and that selecting $W_1 = 0$ and $W_2 = I$ yields the Moore-Penrose inverse.

We use the SR inverse in place of the inverse of B in a PD control law for CMG's. Since the SR inverse introduces error into the inversion, we test the ability of the control law to compensate for this disturbance. The inertia-free control law for CMG's is thus given by the PD-type SO(3)/0 control law

$$u = -Y^{\#}(K_{\mathrm{p}}S + K_{\mathrm{v}}\omega). \tag{45}$$

In the simulations below we do not modify the weight matrices W_1 and W_2 based on the distance of Y from singularity. Alternative methods, such as the singular-direction avoidance (SDA) inverse [49], can also be applied.

V.   FGAC Examples

A.   FGAC Examples Using Thrusters

For all of the examples in this section, we assume that the nominal spacecraft inertia matrix is given by J_3, which corresponds to the centroid in the inertia region shown in Figure 1 with the body-fixed frame assumed to be a principal body-fixed frame. As in

338

Proposition 1, let K_p be given by

$$K_p = \frac{\alpha}{\operatorname{tr} A},$$

(46)

let $K_v = K_v(\omega)$ be given by

$$K_v = \beta \begin{bmatrix} \frac{1}{1+|\omega_1|} & 0 & 0 \\ 0 & \frac{1}{1+|\omega_2|} & 0 \\ 0 & 0 & \frac{1}{1+|\omega_3|} \end{bmatrix},$$

(47)

where $\alpha = \beta = 1$, $K_1 = I_3$, $K_i = 0.015$, and $A = \operatorname{diag}(1, 2, 3)$.

To evaluate performance for R2R examples, we use the settling-time metric

$$k_0 = \min_{k > 100} \{k : \text{ for all } i \in \{1, \dots, 100\}, e((k - i)T_s) < 0.05 \,\text{rad}\},$$

(48)

where k is the simulation step, T_s is the integration step size, and $e(kT_s)$ is the eigenaxis attitude error at the kth simulation step. This metric is thus the minimum time such that the eigenaxis attitude error in the 100 most recent simulation steps is less than 0.05 rad.

To illustrate the inertia-free property of the SO(3)/0 and SO(3)/3 FGAC control laws, the inertia of the spacecraft is varied using

$$J(\alpha) = (1 - \alpha)J_3 + \alpha J_i,$$

(49)

where $\alpha \in [0, 1]$ and $i = 1, 4, 5$. Figure 2 shows how the R2R settling time depends on α.

Next, we investigate robustness to thruster misalignment relative to the principal axes. Here, the inertia matrix is rotated by θ degrees about either the x, y, or z axis. For a rotation about the x axis, J changes according to

$$J = \mathcal{O}_1(\theta) J_i \mathcal{O}_1(\theta)^\mathrm{T},$$

(50)

where $i = 3, 4$. Similar relations exist for rotations about the y and z axes. Figure 3 shows how a thruster misalignment of θ deg affects the settling time, where θ is varied from -180 to +180.

Next, we consider the effect of torque cut-off saturation, that is, where the commanded torque is saturated at the maximum allowable value. Figure 4 shows the effect of increasing saturation levels for SO(3)/0 and SO(3)/3.

Next, we consider R2S maneuvers. As shown in Figure 5, the SO(3)/0 controller cannot stabilize spins unless they are about a principal axis. For a spin about a principal
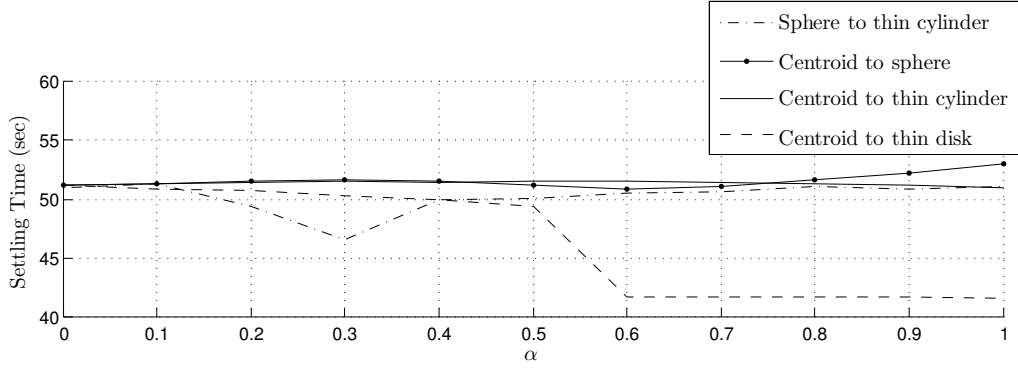
(a)
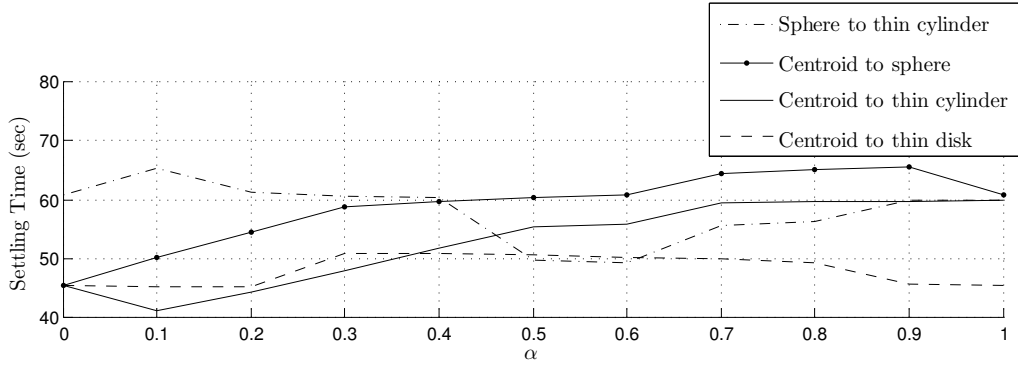
(b)

Figure 2. R2R settling time for the FGAC control laws SO(3)/0 and SO(3)/3 using thrusters as a function of α for various combinations of inertia matrices. The maneuver is 40-deg rotation about the body-fixed direction $[1\ 1\ 1]^{\mathrm{T}}$. Convergence is achieved for (a) SO(3)/0 and (b) SO(3)/3. Each controller is implemented in all cases with a single tuning. In all cases, the spacecraft inertia is unknown.

axis, Euler's equation simplifies to

$$J_{11}\dot{\omega}_1 = (J_{22} - J_{33})\omega_2\omega_3 + u_1, \tag{51}$$

$$J_{22}\dot{\omega}_2 = (J_{33} - J_{11})\omega_1\omega_3 + u_2, \tag{52}$$

$$J_{33}\dot{\omega}_3 = (J_{11} - J_{22})\omega_1\omega_2 + u_3. \tag{53}$$

Therefore, for spins about a principal axis, the equations reduce to a linear second-order system, in which case integrators in the controller are not required to stabilize spin commands, as shown in Figure 5.

As discussed above, SO(3)/0 can stabilize spins about only a principal axis. When the commanded spin is about a non-principal axis, the controller is unable to follow the command as shown in Figure 6.

The SO(3)/3 controller can achieve spins about a non-principal axis, as shown in
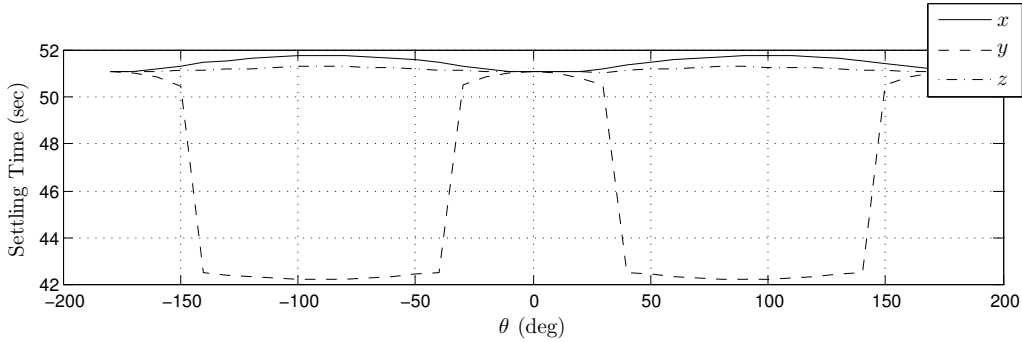
(a)
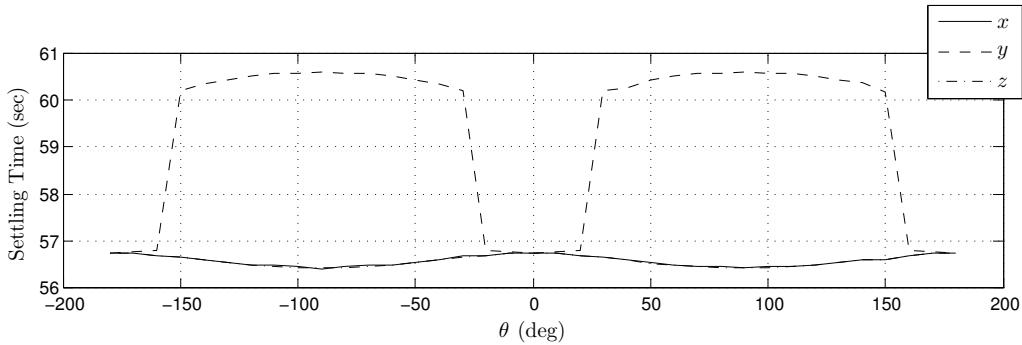
(b)

Figure 3. R2R settling time for the FGAC control laws SO(3)/0 and SO(3)/3 using thrusters as a function of the principal-frame/body-frame rotation angle θ for rotations about each of the three principal axes of J_3. The maneuver is a 40-deg rotation about the body-fixed direction $[1\ 1\ 1]^{\mathrm{T}}$. (a) For the SO(3)/0 controller, variations in the settling time are within 18% of the nominal settling time. (b) For the SO(3)/3 controller, variations in the settling time are within 7% of the nominal settling time.

Figure 7. This controller can also stabilize spins in the presence of a constant torque disturbance, as shown in Figure 8.

B.   FGAC Example Using Magnetic Torquers

We consider a spacecraft in a 450-km circular orbit above the Earth with an inclination of 87 deg. The International Geomagnetic Reference Field (IGRF) model is used to simulate Earth's geomagnetic field as a function of orbital position [44]. The spacecraft inertia matrix J is given by J_3, with the body-fixed frame assumed to be a principal frame.

We use the SO(3)/0 FGAC controller (39) for a M2R maneuver, where the objective is to bring the spacecraft from the initial attitude $R(0) = I_3$, with initial angular velocity $\omega(0) = [0.025\ 0.025\ -0.03]^{\mathrm{T}}$ rad/sec, to rest at the desired final orientation $R_{\mathrm{d}} = I_3$.

(a)   (b)
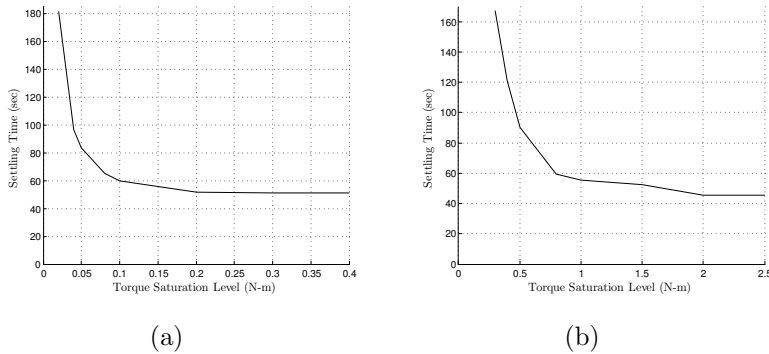
Figure 4. **R2R settling time for the FGAC control laws SO(3)/0 and SO(3)/3 using thrusters as a function of torque for various saturation levels on all three axes, for (a) SO(3)/0 and (b) SO(3)/3. The maneuver is 40-deg rotation about the body-fixed direction $[1\ 1\ 1]^{\mathrm{T}}$. Note that, at low saturation levels, SO(3)/0 stabilizes the spacecraft, whereas SO(3)/3 does not. Saturation does not affect the performance of SO(3)/0 for saturation levels greater than 0.3 N-m.**

Let $K_{\mathrm{p}} = 75$, $K_{\mathrm{v}} = 75$, and $\varepsilon = 0.0004$. These values are chosen to give nominal magnetic dipole moments around 5 A-m^2, and a settling time of around 8 orbits. We test the controller in a nonlinear simulation of (1)-(2).

Figure 9 shows the eigenaxis attitude error, angular velocity, and magnetic dipole moment for the simulation described above. The spacecraft comes to rest at the commanded attitude within 8 orbits. The maximum magnetic dipole moment generated is less than 6 A-m^2. This quantity can be further tuned by modifying the gains K_{p} and K_{v}.

C. FGAC Example Using Reaction Wheels

We now illustrate the effectiveness of the SO(3)/0 FGAC control law (40) for regulating the spacecraft attitude and angular velocity using reaction-wheel actuators. The following spacecraft parameters are assumed. The bus inertia matrix J_{b} is given by the centroid inertia matrix J_3 defined by (10), which is unknown to the controller. The axes of rotation of the reaction wheels are aligned with the spacecraft body-fixed frame unit vectors, and the wheel inertias are given by $J_{\mathrm{w}_1} = \mathrm{diag}(\alpha_1, \beta_1, \beta_1)$ kg-m^2, $J_{\mathrm{w}_2} = \mathrm{diag}(\beta_2, \alpha_2, \beta_2)$ kg-m^2, and $J_{\mathrm{w}_3} = \mathrm{diag}(\beta_3, \beta_3, \alpha_3)$ kg-m^2, where $\alpha_1 = \alpha_2 = \alpha_3 = 1$ and $\beta_1 = \beta_2 = \beta_3 = 0.75$. The values $\beta_1, \beta_2, \beta_3$ are unknown to the controller.

As in Proposition 1, Let K_{p} be given by

$$K_{\mathrm{p}} = \frac{\gamma}{\mathrm{tr}\,A}, \tag{54}$$
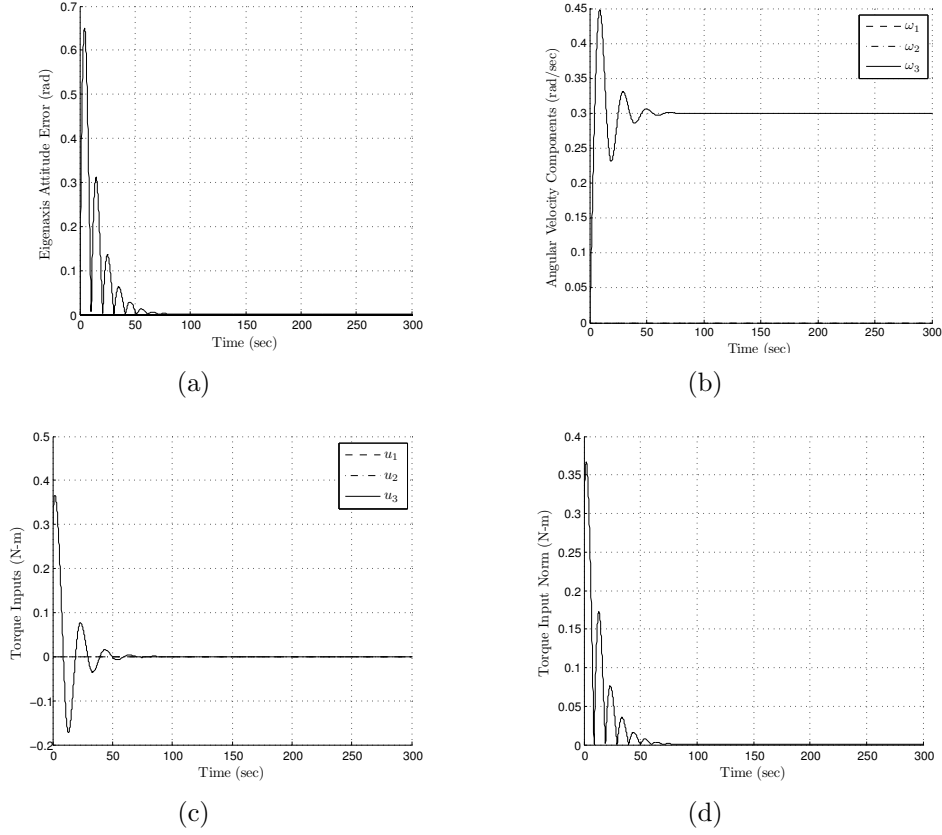
Figure 5. R2S maneuver for the FGAC control law SO(3)/0 using thrusters for $\omega_{\mathrm{d}} = [0\ 0\ 0.3]^{\mathrm{T}}$ rad/sec. (a) Eigenaxis attitude error, (b) angular velocity components, (c) torque inputs, and (d) torque input norm. The spacecraft is initially at rest with $R = I$ and $R_{\mathrm{d}}(0) = I$.

and let $K_{\mathrm{v}} = K_{\mathrm{v}}(\omega)$ be given by

$$
K_{\mathrm{v}} = \eta
\begin{bmatrix}
\frac{1}{1+|\omega_1|} & 0 & 0 \\
0 & \frac{1}{1+|\omega_2|} & 0 \\
0 & 0 & \frac{1}{1+|\omega_3|}
\end{bmatrix},
\tag{55}
$$

where $\gamma = \eta = 15$ and $A = \mathrm{diag}(1, 2, 3)$.

Controller (40) is used for an aggressive slew maneuver, where the objective is to bring the spacecraft from the initial attitude $R_0 = I_3$ and initial angular velocity $\omega(0) = [1\ -1\ 0.5]^{\mathrm{T}}$ rad/sec to rest at the desired final orientation $R_{\mathrm{d}} = \mathrm{diag}(1, -1, -1)$, which represents a rotation of 180 degrees about the x-axis. The reaction wheels are initially not spinning relative to the spacecraft, that is, $\nu(0) = [0\ 0\ 0]^{\mathrm{T}}$ rad/sec. No disturbance is present.

Figures 10(a)-(c) show, respectively, the attitude error, angular-velocity components, and angular-velocity components of the wheels. The spacecraft attitude and

343

(a)

(b)

(c)

(d)
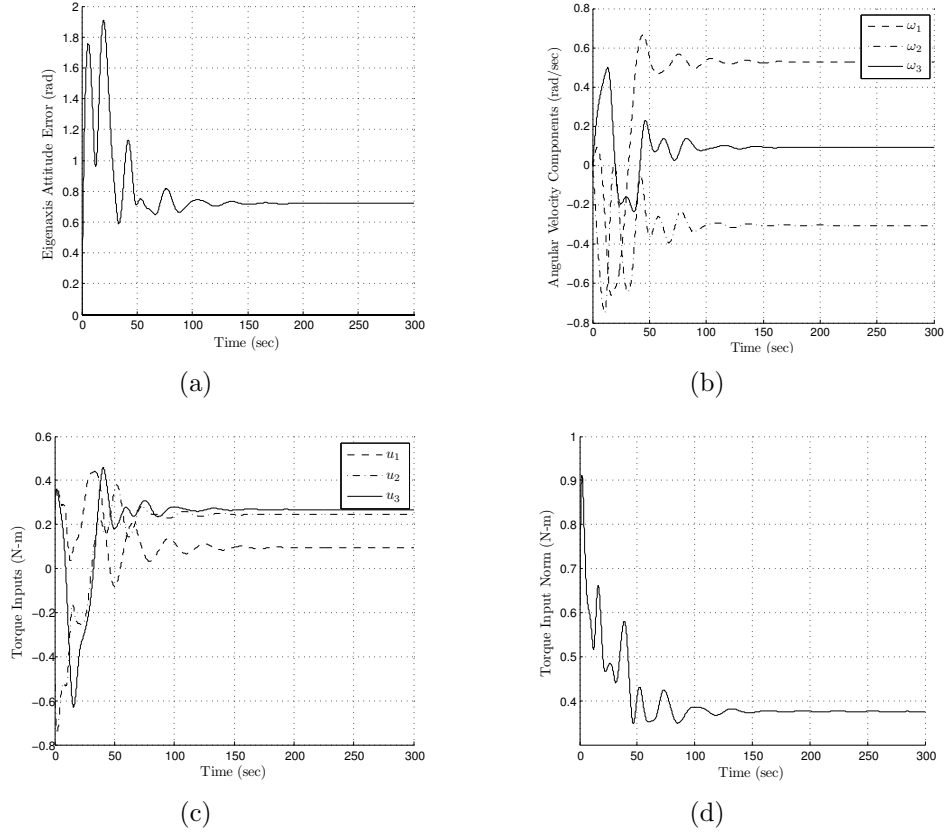
Figure 6. R2S maneuver for the FGAC control law SO(3)/0 using thrusters for $\omega_{\mathrm{d}} = [0.2 \ -0.5 \ 0.3]^{\mathrm{T}}$ rad/sec. (a) Eigenaxis attitude error, (b) angular velocity components, (c) torque inputs, and (d) torque input norm. The spacecraft is initially at rest with $R = I$ and $R_{\mathrm{d}}(0) = I$. The controller spins the spacecraft with the commanded angular rate but about an incorrect axis, as shown by the attitude error.

angular-velocity components reach the commanded values in about 30 sec. The angular-velocity components of the reaction wheels approach constant values that are consistent with the initial, nonzero angular momentum.

D. FGAC Example Using CMG's

We now illustrate the SO(3)/0 FGAC control law (40) using CMG's. The following spacecraft parameters are assumed. The bus inertia matrix J_{b} is given by J_3, which is unknown to the controller. The axes of rotation of the CMG gimbals are aligned with the spacecraft body-fixed frame unit vectors, and the wheel inertias are given by $J_{\mathrm{w}_1} = \mathrm{diag}(\beta_1, \beta_1, \beta_1)$ kg-m^2, $J_{\mathrm{w}_2} = \mathrm{diag}(\beta_2, \beta_2, \beta_2)$ kg-m^2, and $J_{\mathrm{w}_3} = \mathrm{diag}(\beta_3, \beta_3, \beta_3)$ kg-m^2, where $\beta_1 = \beta_2 = \beta_3 = 0.3$.
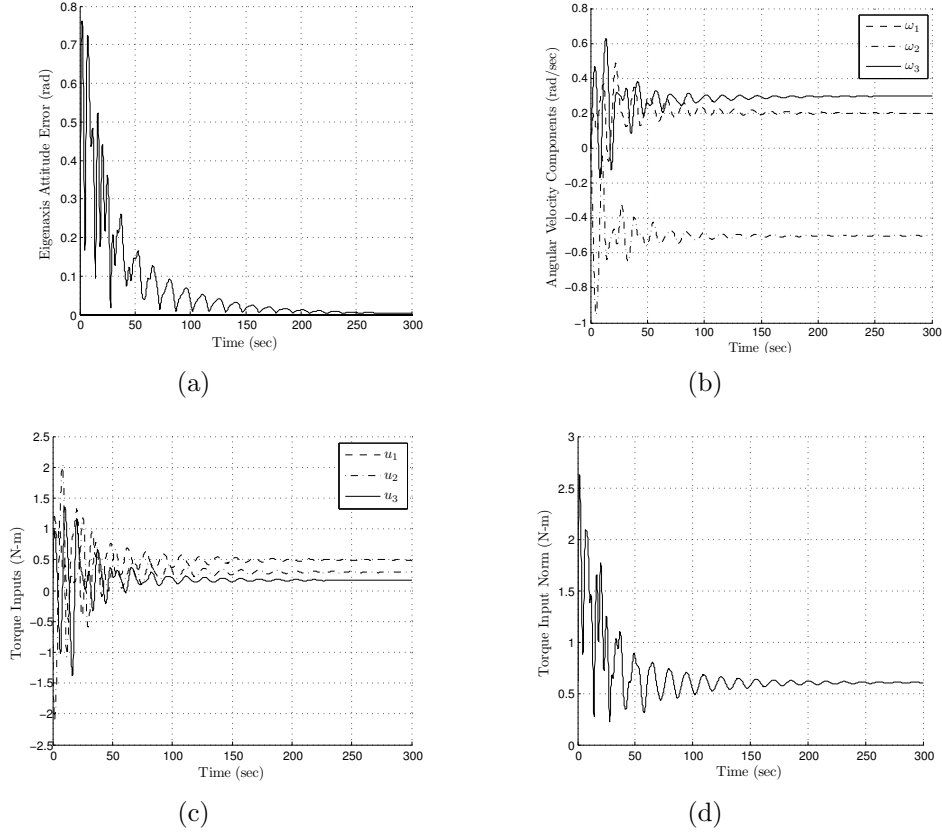
Figure 7. R2S maneuver for the FGAC control law SO(3)/3 using thrusters for $\omega_{\rm d} = [0.2 \ -0.5 \ 0.3]^{\rm T}$ rad/sec. (a) Eigenaxis attitude error, (b) angular-velocity components, (c) torque inputs, and (d) torque input norm. The spacecraft is initially at rest with $R = I$ and $R_{\rm d}(0) = I$.

Let $K_{\rm p}$ be given by

$$K_{\rm p} = 100\frac{\gamma}{{\rm tr}\,A}, \tag{56}$$

and let $K_{\rm v}$ be given by

$$K_{\rm v} = {\rm diag}(100, 100, 100), \tag{57}$$

where $A = {\rm diag}(1, 2, 3)$.

Controller (40) is used for an aggressive slew maneuver, where the objective is to bring the spacecraft from the initial attitude $R_0 = I_3$ and initial angular velocity $\omega(0) = [1 \ -1 \ 0.5]^{\rm T}$ rad/sec to rest at the desired final orientation $R_{\rm d} = {\rm diag}(1, -1, -1)$, which represents a rotation of 180 degrees about the x-axis. The reaction wheels are initially not spinning relative to the spacecraft, that is, $\nu(0) = [0 \ 0 \ 0]^{\rm T}$ rad/sec. No disturbance is present.

Figure 11 shows the attitude error, angular-velocity components, gimbal angles, and

345
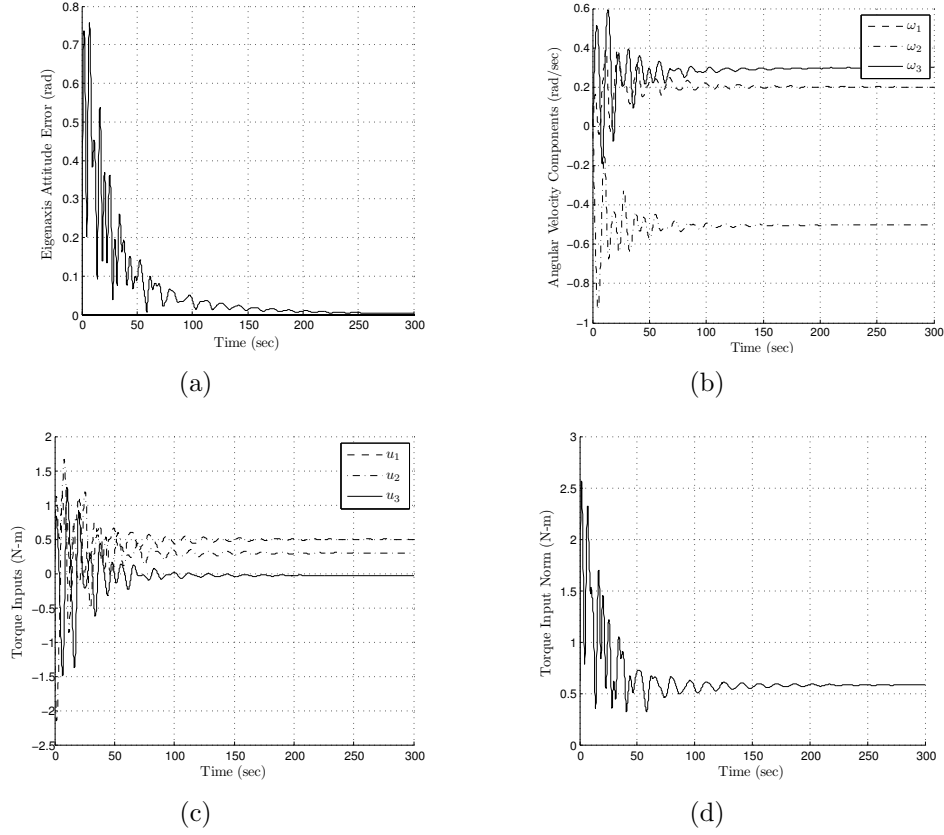
Figure 8. R2S maneuver for the FGAC control law SO(3)/3 using thrusters for $\omega_{\mathrm{d}} = [0.2 \ -0.5 \ 0.3]^{\mathrm{T}}$ rad/sec in the presence of the constant disturbance torque $d = [0 \ 0 \ 0.2]^{\mathrm{T}}$ N-m. (a) Eigenaxis attitude error, (b) angular velocity components, (c) torque inputs, and (d) torque input norm. The spacecraft is initially at rest with $R = I$ and $R_{\mathrm{d}}(0) = I$. The controller is able to reject the disturbance and follow the spin command.

singular values of B. The spacecraft attitude and angular-velocity components reach the commanded values in about 10 sec. The relative angular-velocity components of the reaction wheels settle down to constant values that are consistent with the initial, nonzero angular momentum.

VI.   Estimator-Based Attitude Control (EBAC)

The main difference between the EBAC control laws and the FGAC control laws is that the latter exploit an estimate of the inertia matrix. These control laws are based on Lyapunov analysis, which also provides disturbance rejection for harmonic disturbances with known spectrum.
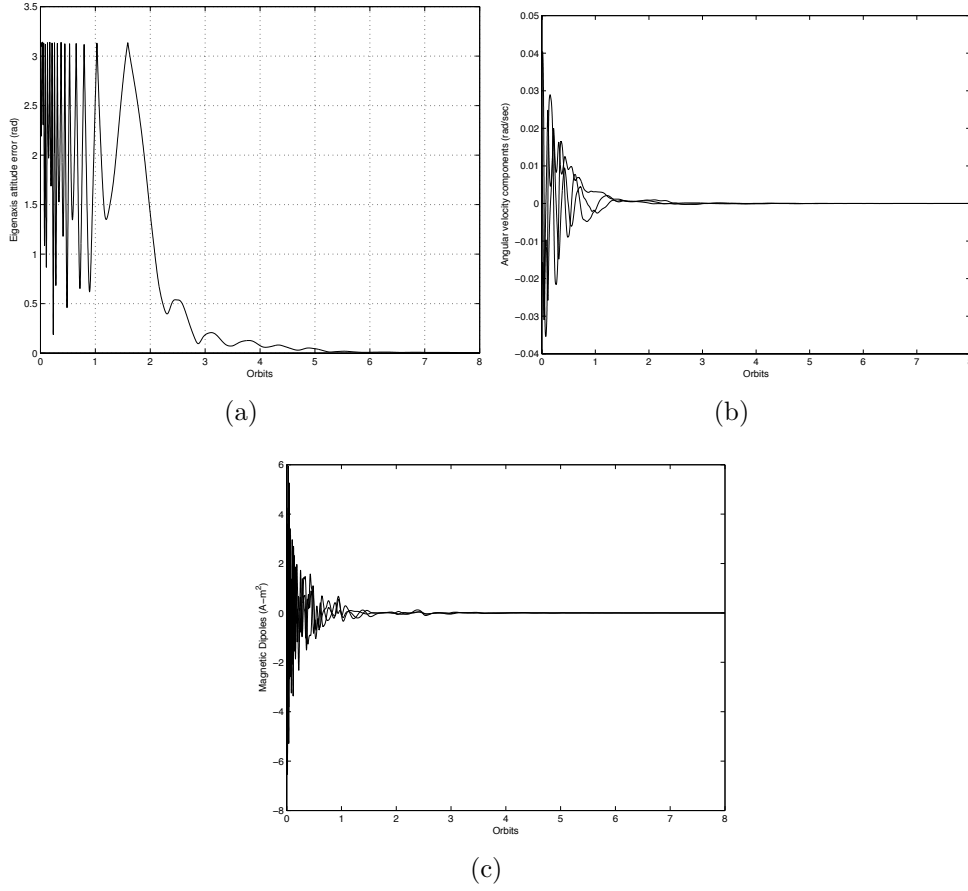
Figure 9. M2R maneuver for the FGAC control law (39) using magnetic torquers. (a) Eigenaxis attitude error, (b) angular velocity components, and (c) magnetic dipole moments. The spacecraft comes to rest at the commanded attitude within 7 orbits, and the maximum magnetic dipole moment required by the controller is less than 6 A-m^2.

A. EBAC for Thrusters

To develop an estimate of the spacecraft inertia, we introduce the notation

$$Jw = L(\omega)\gamma, \tag{58}$$

where $\gamma \in \mathbb{R}^6$ is defined by

$$\gamma \triangleq \begin{bmatrix} J_{11} & J_{22} & J_{33} & J_{23} & J_{13} & J_{12} \end{bmatrix}^{\mathrm{T}}$$

and

$$L(\omega) \triangleq \begin{bmatrix} \omega_1 & 0 & 0 & 0 & \omega_3 & \omega_2 \\ 0 & \omega_2 & 0 & \omega_3 & 0 & \omega_1 \\ 0 & 0 & \omega_3 & \omega_2 & \omega_1 & 0 \end{bmatrix}.$$

347

(a)

(b)

(c)
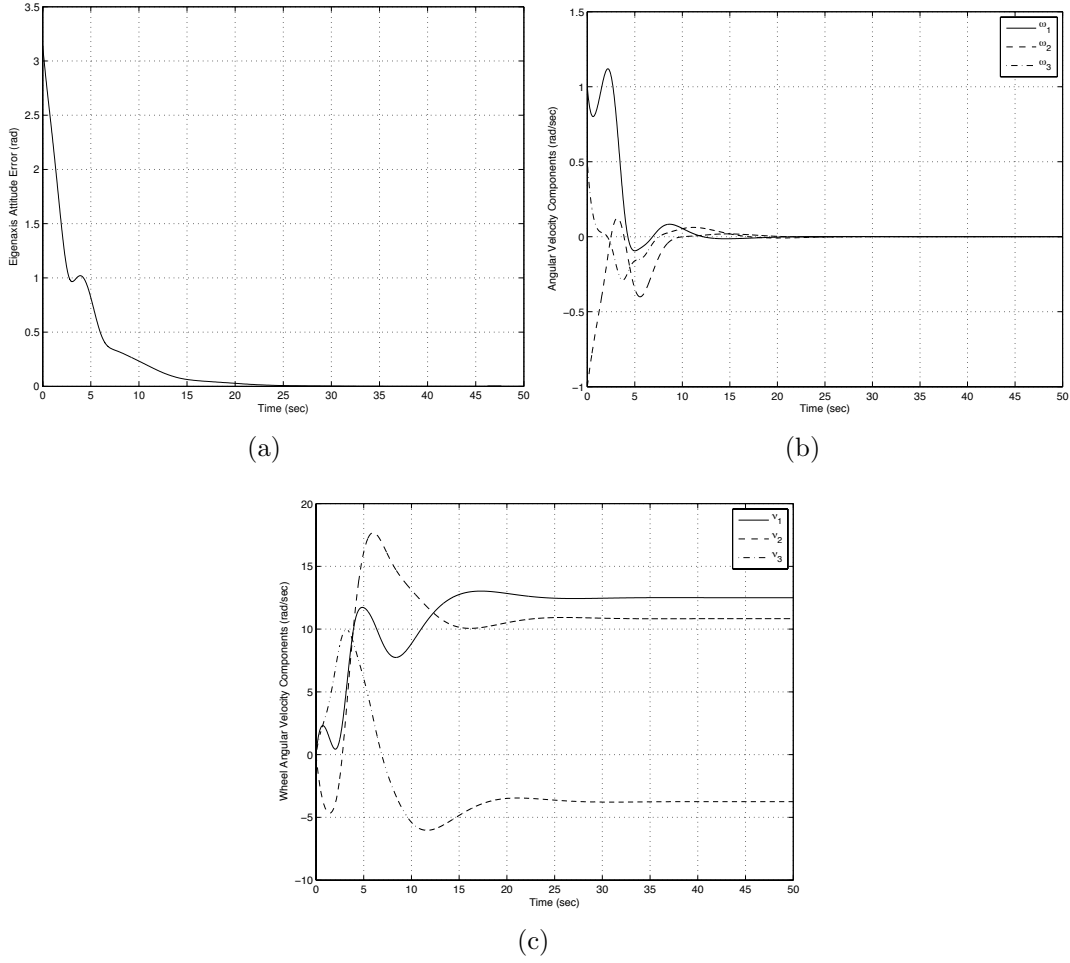
Figure 10. M2S maneuver for the FGAC control law (40) using reaction wheels and without disturbance. (a) Eigenaxis error, (b) spacecraft angular velocity components, and (c) wheel angular velocity components. The objective is to bring the spacecraft from the initial attitude $R(0) = I_3$ and initial angular velocity $\omega(0) = [1 \quad -1 \quad 0.5]^{\mathrm{T}}$ rad/sec to rest at the desired final orientation $R_{\mathrm{d}} = \mathrm{diag}(1, -1, -1)$, which represents a rotation of 180 degrees about the x-axis.

With this notation, (73) can be rewritten as

$$J\dot{\tilde{\omega}} = [L(\tilde{\omega} + \tilde{R}^{\mathrm{T}}\omega_{\mathrm{d}})\gamma]^{\times}(\tilde{\omega} + \tilde{R}^{\mathrm{T}}\omega_{\mathrm{d}}) + L(\tilde{\omega} \times \tilde{R}^{\mathrm{T}}\omega_{\mathrm{d}} - \tilde{R}^{\mathrm{T}}\dot{\omega}_{\mathrm{d}})\gamma + Bu + z_{\mathrm{dist}}. \qquad (59)$$

Next, let $\hat{J} \in \mathbb{R}^{3\times3}$ denote an estimate of J, and define the inertia-estimation error

$$\tilde{J} \triangleq J - \hat{J}.$$

Letting $\hat{\gamma}, \tilde{\gamma} \in \mathbb{R}^6$ represent $\hat{J}, \tilde{J}$, respectively, it follows that

$$\tilde{\gamma} = \gamma - \hat{\gamma}. \qquad (60)$$

348

(a)

(b)

(c)

(d)
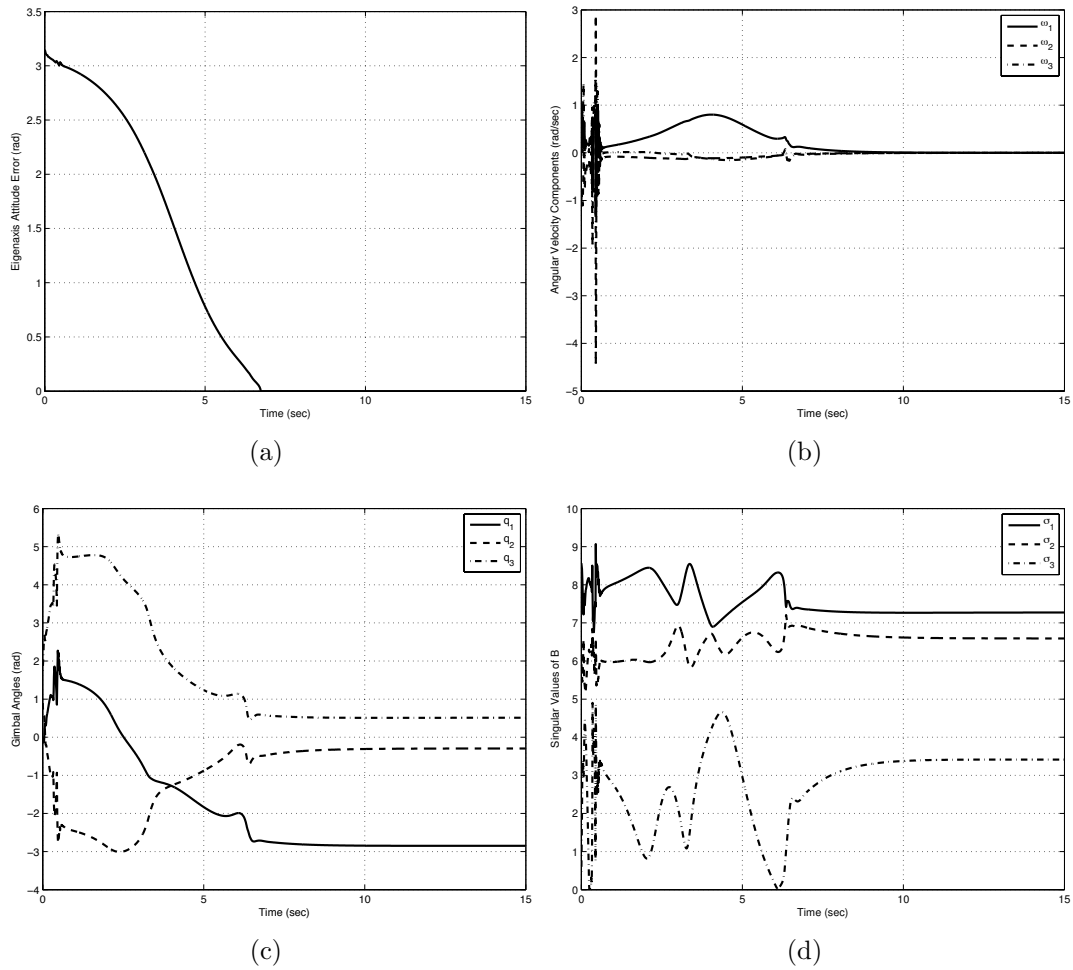
Figure 11. M2R maneuver for the FGAC control law (45) using CMGs and without disturbance. (a) Eigenaxis error, (b) spacecraft angular velocity components, (c) gimbal angles, and (d) singular values of B. the objective is to bring the spacecraft from the initial attitude $R(0) = I_3$ and initial angular velocity $\omega(0) = [1 \;\; -1 \; 0.5]^{\mathrm{T}}$ rad/sec to rest at the desired final orientation $R_{\mathrm{d}} = \mathrm{diag}(1, -1, -1)$, which represents a rotation of 180 degrees about the x-axis.

Likewise, let $\hat{z}_{\text{dist}} \in \mathbb{R}^3$ denote an estimate of z_{dist}, and define the disturbance-estimation error

$$\tilde{z}_{\text{dist}} \stackrel{\triangle}{=} z_{\text{dist}} - \hat{z}_{\text{dist}}.$$

Assuming that the disturbance is harmonic, it follows that z_{dist} can be modeled as the output of an autonomous system of the form

$$\dot{d} = A_d d, \tag{61}$$
$$z_{\text{dist}} = C_d d, \tag{62}$$

where $A_d \in \mathbb{R}^{n_d \times n_d}$ and $C_d \in \mathbb{R}^{3 \times n_d}$ are known matrices and A_d is a Lyapunov-stable matrix. In this model, $d(0)$ is unknown, which is equivalent to the assumption that the amplitude and phase of all harmonic components in the disturbance are unknown. The matrix A_d is chosen to include eigenvalues of all frequency components that may be present in the disturbance signal, where the zero eigenvalue corresponds to constant disturbances. In effect, the controller provides infinite gain at the disturbance frequency, which results in asymptotic rejection of harmonic disturbance components. In particular, an integral controller provides infinite gain at DC in order to reject constant disturbances. In the case of orbit-dependent disturbances, the frequencies can be estimated from the orbital parameters. Likewise, in the case of disturbances originating from on-board devices, the spectral content of the disturbances may be known. In other cases, it may be possible to estimate the spectrum of the disturbances through signal processing. Since z_{d} is harmonic, A_d can be chosen to be skew symmetric, which we do henceforth. Let $\hat{d} \in \mathbb{R}^{n_d}$ denote an estimate of d, and define the disturbance-state estimation error

$$\tilde{d} \stackrel{\triangle}{=} d - \hat{d}.$$

Theorem 1. Let K_{p} be a positive number, let $K_1 \in \mathbb{R}^{3 \times 3}$, let $Q \in \mathbb{R}^{6 \times 6}$ and $D \in \mathbb{R}^{n_d \times n_d}$ be positive definite, let $A = \text{diag}(a_1, a_2, a_3)$ be a diagonal positive-definite matrix, and define

$$S \stackrel{\triangle}{=} \sum_{i=1}^{3} a_i (\tilde{R}^{\text{T}} e_i) \times e_i.$$

Then the Lyapunov candidate

$$V(\tilde{\omega}, \tilde{R}, \tilde{\gamma}, \tilde{d}) \stackrel{\triangle}{=} \tfrac{1}{2}(\tilde{\omega} + K_1 S)^{\text{T}} J(\tilde{\omega} + K_1 S) + K_{\text{p}} \text{tr}\,(A - A\tilde{R}) + \tfrac{1}{2}\tilde{\gamma}^{\text{T}} Q\tilde{\gamma} + \tfrac{1}{2}\tilde{d}^{\text{T}} D\tilde{d} \tag{63}$$

is positive definite, that is, V is nonnegative, and $V = 0$ if and only if $\tilde{\omega} = 0$, $\tilde{R} = I$, $\tilde{\gamma} = 0$, and $\tilde{d} = 0$.

Theorem 2. Let K_{p} be a positive number, let $K_{\text{v}} \in \mathbb{R}^{3 \times 3}$, $K_1 \in \mathbb{R}^{3 \times 3}$, $Q \in \mathbb{R}^{6 \times 6}$, and $D \in \mathbb{R}^{n_d \times n_d}$ be positive definite, assume that $A_d^{\text{T}} D + DA_d$ is negative semidefinite, let $A = \text{diag}(a_1, a_2, a_3)$ be a diagonal positive-definite matrix, define S and V as in

Theorem 1, and let $\hat{\gamma}$ and $\hat{d}$ satisfy

$$\dot{\hat{\gamma}} = Q^{-1}[L^{\mathrm{T}}(\omega)\omega^{\times} + L^{\mathrm{T}}(K_1\dot{S} + \tilde{\omega} \times \omega - \tilde{R}^{\mathrm{T}}\dot{\omega}_{\mathrm{d}})](\tilde{\omega} + K_1 S), \tag{64}$$

where

$$\dot{S} = \sum_{i=1}^{3} a_i[(\tilde{R}^{\mathrm{T}}e_i) \times \tilde{\omega}] \times e_i, \tag{65}$$

and

$$\dot{\hat{d}} = A_d \hat{d} + D^{-1}C_d^{\mathrm{T}}(\tilde{\omega} + K_1 S), \tag{66}$$

$$\hat{z}_{\mathrm{dist}} = C_d \hat{d}. \tag{67}$$

Furthermore, let

$$u = B^{-1}(v_1 + v_2 + v_3), \tag{68}$$

where

$$v_1 \triangleq -(\hat{J}\omega) \times \omega - \hat{J}(K_1\dot{S} + \tilde{\omega} \times \omega - \tilde{R}^{\mathrm{T}}\dot{\omega}_{\mathrm{d}}), \tag{69}$$

$$v_2 \triangleq -\hat{z}_{\mathrm{dist}}, \tag{70}$$

and

$$v_3 \triangleq -K_{\mathrm{v}}(\tilde{\omega} + K_1 S) - K_{\mathrm{p}}S. \tag{71}$$

Then,

$$\dot{V}(\tilde{\omega}, \tilde{R}, \tilde{\gamma}, \tilde{d}) = -(\tilde{\omega} + K_1 S)^{\mathrm{T}}K_{\mathrm{v}}(\tilde{\omega} + K_1 S) - K_{\mathrm{p}}S^{\mathrm{T}}K_1 S + \tfrac{1}{2}\tilde{d}^{\mathrm{T}}(A_d^{\mathrm{T}}D + DA_d)\tilde{d} \tag{72}$$

is negative semidefinite.

The closed-loop spacecraft attitude dynamics have the form

$$J\dot{\tilde{\omega}} = [J(\tilde{\omega} + \tilde{R}^{\mathrm{T}}\omega_{\mathrm{d}})] \times (\tilde{\omega} + \tilde{R}^{\mathrm{T}}\omega_{\mathrm{d}}) + J(\tilde{\omega} \times \tilde{R}^{\mathrm{T}}\omega_{\mathrm{d}} - \tilde{R}^{\mathrm{T}}\dot{\omega}_{\mathrm{d}}) + \tau_{\mathrm{actuators}} + z_{\mathrm{dist}}, \tag{73}$$

and the control law (68)-(71) can be expressed as

$$J\dot{\tilde{\omega}} = [L(\omega)\tilde{\gamma}]^{\times}\omega + L(\tilde{\omega} \times \tilde{R}^{\mathrm{T}}\omega_{\mathrm{d}} - R^{\mathrm{T}}\dot{\omega}_{\mathrm{d}})\tilde{\gamma} - L(K_1\dot{S})\hat{\gamma} + \tilde{z}_{\mathrm{dist}} - K_{\mathrm{v}}(\tilde{\omega} + K_1 S) - K_{\mathrm{p}}S. \tag{74}$$

From Lemma 3 and Lemma 4 of [22], the closed-loop system consisting of (64)-(67) and (74) has four disjoint equilibrium manifolds. These equilibrium manifolds in $\mathbb{R}^3 \times$

$SO(3) \times \mathbb{R}^6 \times \mathbb{R}^3$ are given by

$$\mathcal{E}_i = \left\{ (\tilde{\omega}, \tilde{R}, \tilde{\gamma}, \tilde{d}) \in \mathbb{R}^3 \times SO(3) \times \mathbb{R}^6 \times \mathbb{R}^3 : \tilde{R} = \mathcal{R}_i, \ \tilde{\omega} \equiv 0, \ (\tilde{\gamma}, \tilde{d}) \in \mathcal{Q}_i \right\}, \qquad (75)$$

where, for all $i \in \{0, 1, 2, 3\}$, $\mathcal{Q}_i$ is the closed subset of $\mathbb{R}^6 \times \mathbb{R}^3$ defined by

$$\mathcal{Q}_i \triangleq \{ (\tilde{\gamma}, \tilde{d}) \in \mathbb{R}^6 \times \mathbb{R}^3 : [L(\mathcal{R}_i^{\mathrm{T}} \omega_{\mathrm{d}}) \tilde{\gamma}]^\times (\mathcal{R}_i^{\mathrm{T}} \omega_{\mathrm{d}}) - L(\mathcal{R}_i^{\mathrm{T}} \dot{\omega}_{\mathrm{d}}) \tilde{\gamma} + C_d \tilde{d} = 0, \ \dot{\tilde{\gamma}} = 0, \ \dot{\tilde{d}} = A_d \tilde{d} \}.$$

Furthermore, the equilibrium manifold $(\tilde{\omega}, \tilde{R}, (\tilde{\gamma}, \tilde{d})) = (0, I, \mathcal{Q}_0)$ of the closed-loop system given by (64)-(67) and (74) is locally asymptotically stable, and the remaining equilibrium manifolds given by $(0, \mathcal{R}_i, \mathcal{Q}_i)$, for $i \in \{1, 2, 3\}$ are unstable. Finally, the set of all initial conditions converging to these equilibrium manifolds forms a lower dimensional submanifold of $\mathbb{R}^3 \times SO(3) \times \mathbb{R}^6 \times \mathbb{R}^3$. $\qquad \square$

Saturation techniques for the EBAC controller are discussed in [29].

B. EBAC for Reaction Wheels

We invoke the same assumptions presented in Section IV.C. The EBAC controller for reaction-wheel actuators is given by [27]

$$u = -J_\alpha^{-1}(v_1 + v_2 + v_3), \qquad (76)$$

where

$$v_1 \triangleq -(\hat{J}_{\mathrm{sc}}\omega + J_\alpha \nu) \times \omega - \hat{J}_{\mathrm{sc}}(K_1 \dot{S} + \tilde{\omega} \times \omega - \tilde{R}^{\mathrm{T}} \dot{\omega}_{\mathrm{d}}), \qquad (77)$$

and v_2, v_3 remain unchanged and are given by (70)-(71). Similarly, the Lyapunov function (63) and its derivative (72) are the same. As in the FGAC case, this control law does not regulate the speed of the wheels, so the function V is not a positive-definite function of the angular velocities of the wheels relative to the bus.

C. EBAC for CMG's

As in the reaction-wheel case, we invoke the assumptions presented in Section IV.D. The EBAC controller for CMG's is given by [28]

$$u = B^\#(v_1 + v_2 + v_3), \qquad (78)$$

where $B^\#$ is the SR-inverse of B,

$$v_1 \triangleq -(\hat{J}_{\mathrm{sc}}\omega + \sum_{i=1}^{3} \beta_i \omega_{\mathrm{W}_i}) \times \omega - \hat{J}_{\mathrm{sc}}(K_1 \dot{S} + \tilde{\omega} \times \omega - \tilde{R}^{\mathrm{T}} \dot{\omega}_{\mathrm{d}}), \qquad (79)$$

and v_2, v_3 remain unchanged and are given by (70)-(71).

VII. EBAC Examples

A. EBAC Examples Using Thrusters

We illustrate two EBAC control laws using thrusters. SO(3)/6 is obtained from the EBAC control law (68) by specializing $u = B^{-1}(v_1 + v_3)$ and SO(3)/9 is given by (68).

To illustrate the inertia-free property of the SO(3)/6 and SO(3)/9 FGAC control laws, the inertia of the spacecraft is varied using (49), where $\alpha \in [0, 1]$ and $i = 1, 4, 5$. Figure 12 shows how the R2R settling time depends on α.
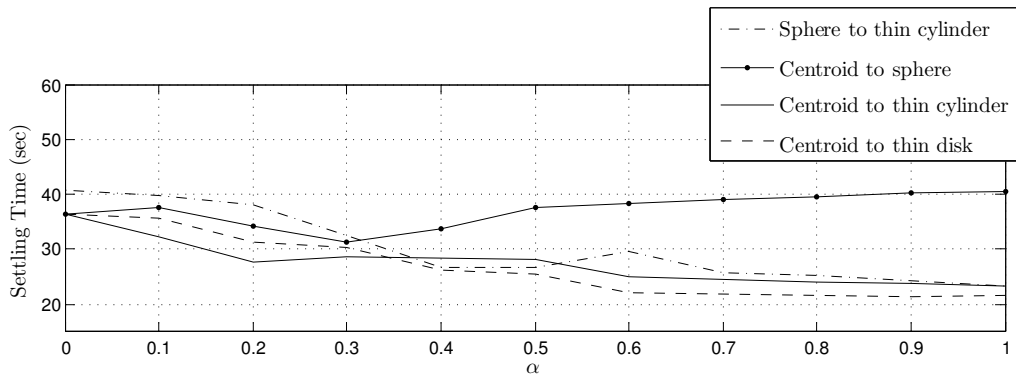
(a)
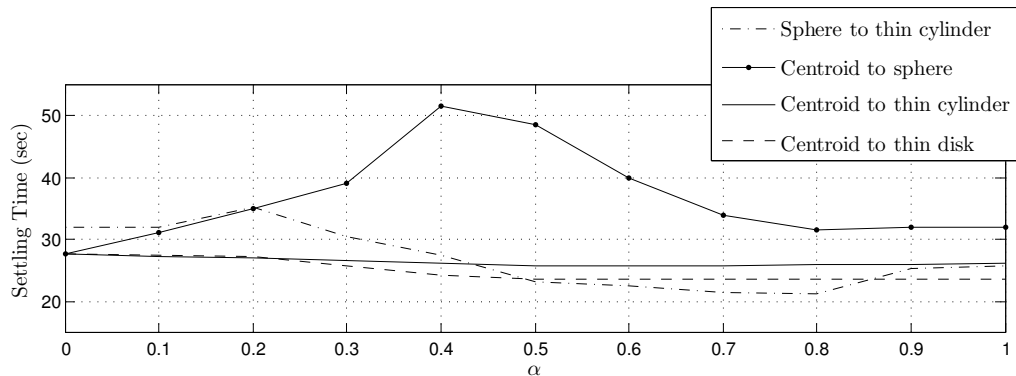
(b)

Figure 12. R2R settling time for the EBAC control laws SO(3)/6 and SO(3)/9 using thrusters as a function of α for various combinations of inertia matrices. The maneuver is 40-deg rotation about the body-fixed direction $[1\ 1\ 1]^{\mathrm{T}}$. Convergence is achieved for (a) SO(3)/6 and (b) SO(3)/9. Each controller is implemented in all cases with a single tuning.

Robustness in relation to thruster misalignment is also tested, and the results are shown in Figures 13 and 14. Simulations are performed using both J_3 and J_4.

Figure 14 shows how thruster misalignment affects the spacecraft with inertia J_1.

We also test the effect of saturation on the EBAC control laws SO(3)/6 and SO(3)/9,
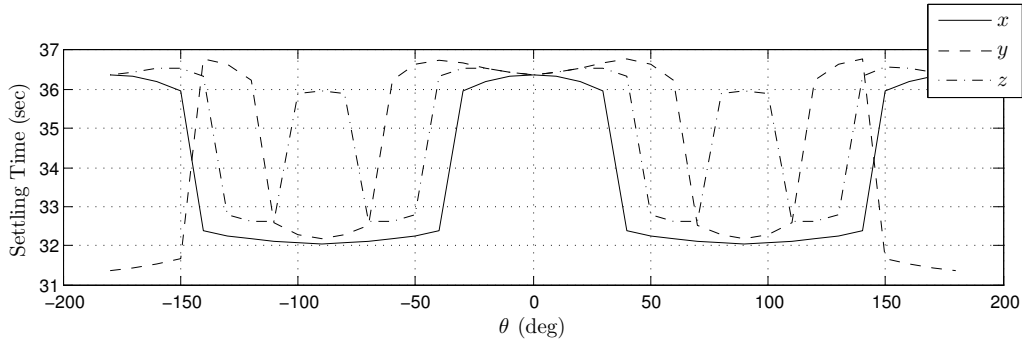
(a)
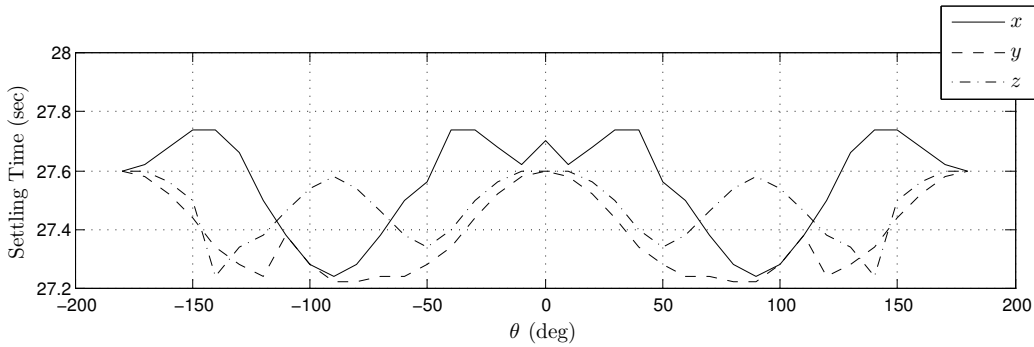
(b)

Figure 13. R2R settling time for the EBAC control laws SO(3)/6 and SO(3)/9 using thrusters as a function of the principal-frame/body-frame rotation angle θ for rotations about each of the three principal axes of J_3. The maneuver is a 40-deg rotation about the body-fixed direction $[1\ 1\ 1]^{\mathrm{T}}$. (a) For the SO(3)/6 controller, variations in the settling time are within 15% of the nominal settling time. (b) For the SO(3)/9 controller, variations in the settling time are within 2% of the nominal settling time.

for various inertia cases. Figure 15 shows that SO(3)/6 and SO(3)/9 are more sensitive to saturation than the FGAC control laws SO(3)/0 and SO(3)/3.

Figure 16 and Figure 17 illustrate how the EBAC and FGAC control laws handle disturbance torques about the minor axis. Note that the SO(3)/0 and SO(3)/6 control laws cannot reject constant disturbances.

Figure 18 shows that the SO(3)/6 controller is able to follow spin commands about a non-principal axis, albeit with large settling times.

As illustrated in Figure 19, in the presence of a disturbance, the SO(3)/6 EBAC control law cannot follow spin commands, and the resulting spin is about an incorrect axis.

The SO(3)/9 EBAC control law can perform R2S maneuvers, as shown in Figure 20. The controller can also stabilize spins with constant disturbance torques as shown

(a)

(b)

Figure 14. R2R settling time for the EBAC control laws SO(3)/6 and SO(3)/9 using thrusters as a function of the principal-frame/body-frame rotation angle θ for rotations about each of the three principal axes of J_4. The maneuver is a 40-deg rotation about the body-fixed direction $[1\ 1\ 1]^{\mathrm{T}}$. (a) For the SO(3)/6 controller, variations in the settling time are within 14% of the nominal settling time. (b) For the SO(3)/9 controller, variations in the settling time are within 18% of the nominal settling time.

in Figure 21.

Next, we consider a gravity gradient disturbance torque τ_{g} modeled by [30, pp. 386–390]

$$\tau_g = 3n^2(\mathcal{O}_{\mathrm{SC/L}}e_3)^\times J(\mathcal{O}_{\mathrm{SC/L}}e_3), \tag{80}$$

where $n \overset{\triangle}{=} \sqrt{\mu/r_{\mathrm{E}}^3}$ is the orbital angular velocity, μ is the gravitational parameter, r_{E} is the Earth radius, e_3 is the third column of the 3×3 identity matrix, and $\mathcal{O}_{\mathrm{SC/L}} \in \mathbb{R}^{3\times3}$ is the orientation matrix of the spacecraft frame $\mathrm{F_{SC}}$ relative to the local-vertical-local-horizontal frame $\mathrm{F_L}$. We assume that the satellite orbit is circular and equatorial.

Rotating the inertial frame $\mathrm{F_{In}}$ about the z-axis by $\pi/2$ rad, then about x-axis by

Figure 15. R2R settling time for the EBAC control laws SO(3)/6 and SO(3)/9 using thrusters as a function of torque for saturation on all three axes using the inertia matrices (a) centroid, (b) sphere, (c) thin disk, and (d) thin cylinder . The maneuver is 40-deg rotation about the body-fixed direction $[1\ 1\ 1]^{\mathrm{T}}$. Note that convergence improves as the saturation level increases.
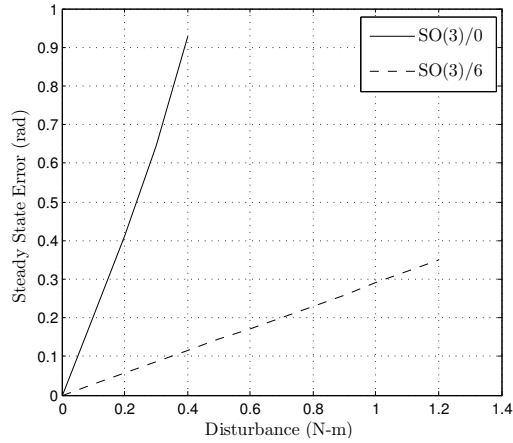
Figure 16. R2R steady-state error for the EBAC control law SO(3)/6 using thrusters as a function of the magnitude of a constant disturbance about the minor axis. The maneuver is a 40-deg rotation about the body-fixed direction $[1\ 1\ 1]^{\mathrm{T}}$. Note that the performance of SO(3)/6 is substantially better than the performance of SO(3)/0.
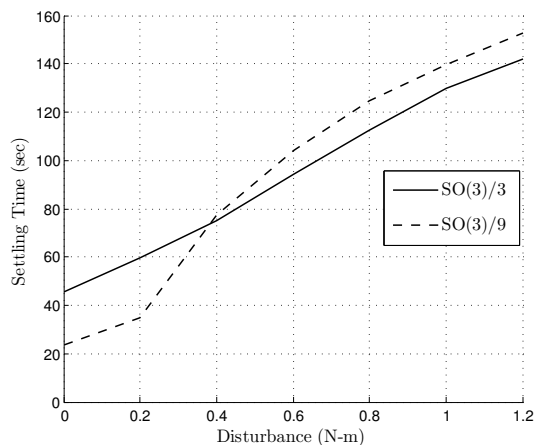
Figure 17. R2R settling time for the EBAC control laws SO(3)/3 and SO(3)/9 using thrusters as a function of the magnitude of a constant torque disturbance about the minor axis. The maneuver is 40-deg rotation about the body-fixed direction $[1\ 1\ 1]^{\mathrm{T}}$. Note that the performance of SO(3)/3 improves in relation to SO(3)/9 as the magnitude of the disturbance increases.
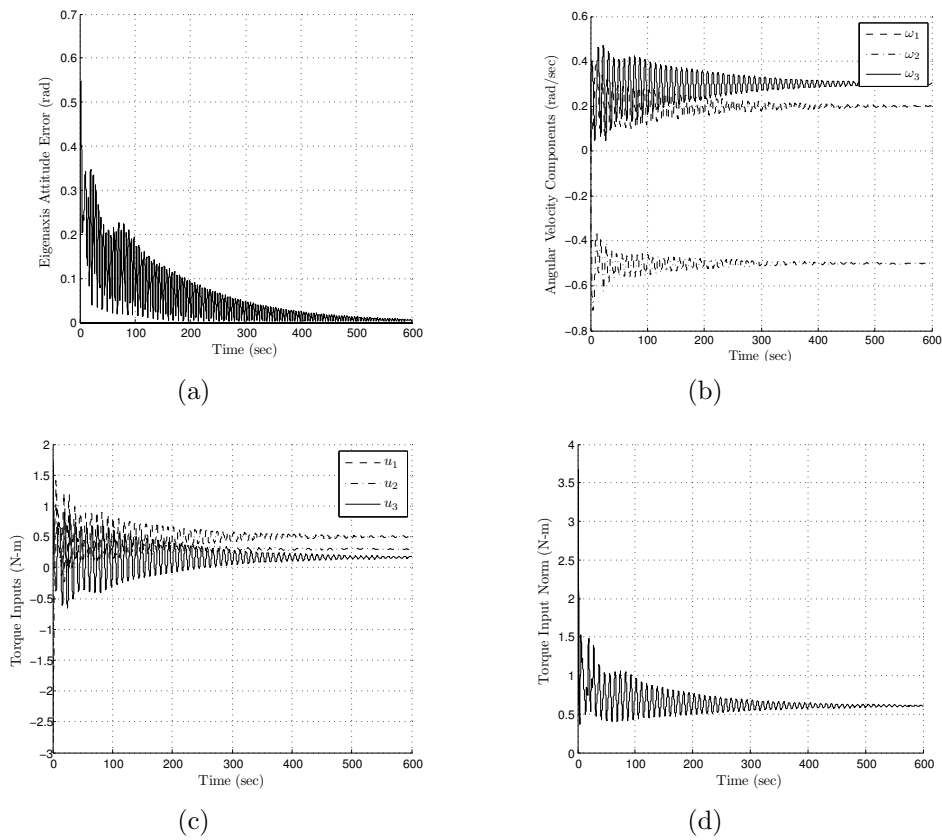
Figure 18. **R2S maneuver for the EBAC control law SO(3)/6 using thrusters for** $\omega_{\mathrm{d}} = [0.2 \ -0.5 \ 0.3]^{\mathrm{T}}$ **rad/sec. (a) Eigenaxis attitude error, (b) angular-velocity components, (c) torque inputs, and (d) torque input norm. The spacecraft is initially at rest with** $R = I$ **and** $R_{\mathrm{d}}(0) = I$**.**

(a)

(b)

(c)

(d)
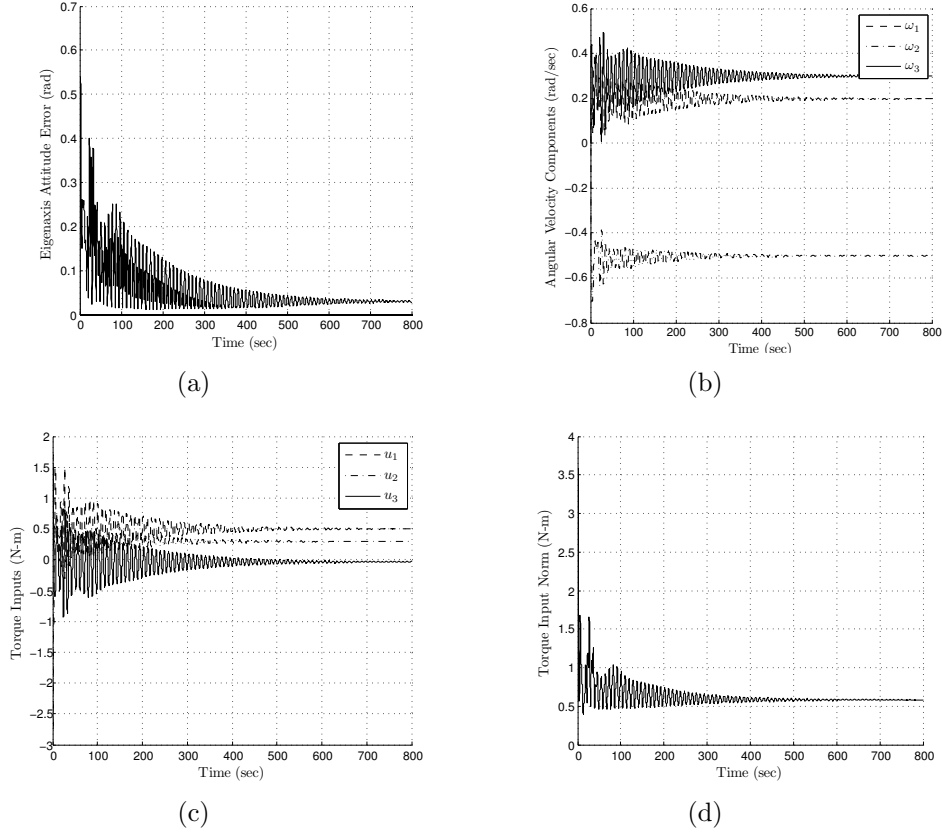
Figure 19. R2S maneuver for the EBAC control law SO(3)/6 using thrusters for $\omega_{\mathrm{d}} = [0.2 \ -0.5 \ 0.3]^{\mathrm{T}}$ rad/sec in the presence of a constant disturbance torque $d = [0 \ 0 \ 0.2]^{\mathrm{T}}$ N-m. (a) Eigenaxis attitude error, (b) angular velocity components, (c) torque inputs, and (d) torque input norm. The spacecraft is initially at rest with $R = I$ and $R_{\mathrm{d}}(0) = I$. The controller cannot reject the disturbance and the resulting spin is about an incorrect axis.

$-\pi/2$ rad, and, finally, about y-axis by $-nt$ rad, $\mathcal{O}_{\mathrm{In/L}}$ is given by

$$\mathcal{O}_{\mathrm{In/L}} = \begin{bmatrix} \sin(nt) & 0 & -\cos(nt) \\ -\cos(nt) & 0 & -\sin(nt) \\ 0 & 1 & 0 \end{bmatrix}. \tag{81}$$

Furthermore, $\mathcal{O}_{\mathrm{SC/L}} = \mathcal{O}_{\mathrm{SC/In}}\mathcal{O}_{\mathrm{In/L}}$. If the body frame is a principal-axis frame, then the gravity gradient disturbance torque τ_g is given by

$$\tau_g = 3n^2 \begin{bmatrix} -(J_{22} - J_{33})\mathcal{O}_{\mathrm{SC/L}_{23}}\mathcal{O}_{\mathrm{SC/L}_{33}} \\ -(J_{33} - J_{11})\mathcal{O}_{\mathrm{SC/L}_{33}}\mathcal{O}_{\mathrm{SC/L}_{13}} \\ -(J_{11} - J_{22})\mathcal{O}_{\mathrm{SC/L}_{13}}\mathcal{O}_{\mathrm{SC/L}_{23}} \end{bmatrix}, \tag{82}$$

where J_{11}, J_{22}, J_{33} are the diagonal entries of J and $[\mathcal{O}_{\mathrm{SC/L}_{13}} \ \mathcal{O}_{\mathrm{SC/L}_{23}} \ \mathcal{O}_{\mathrm{SC/L}_{33}}]^{\mathrm{T}}$ is the third column of $\mathcal{O}_{\mathrm{SC/L}}$.
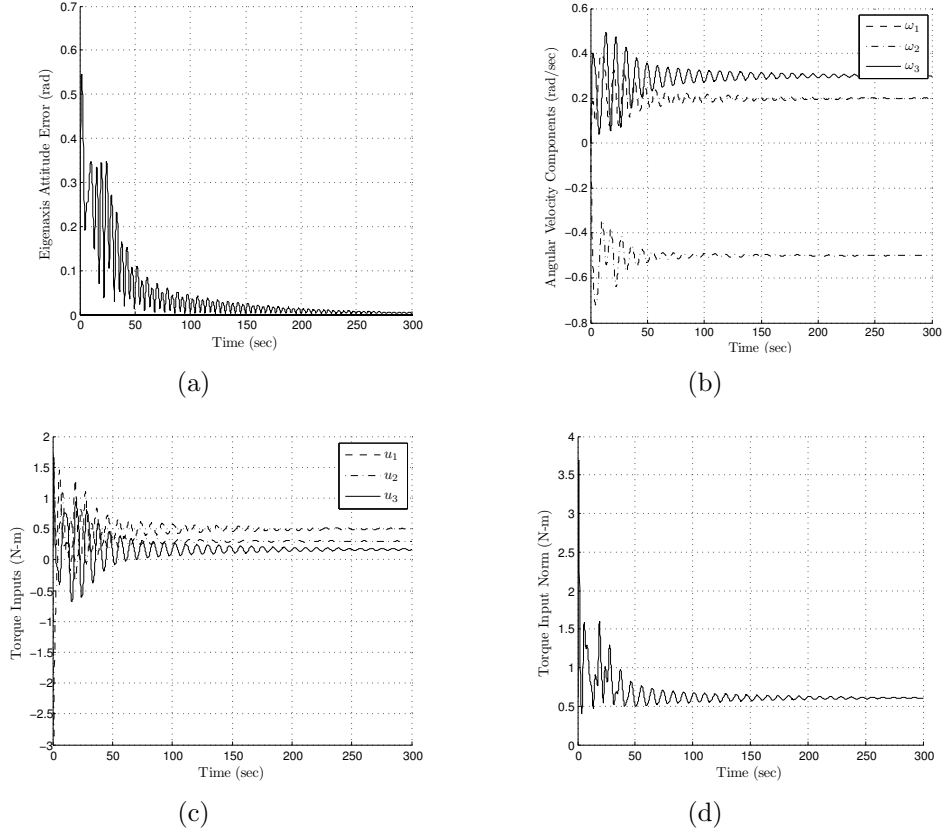
Figure 20. R2S maneuver for the EBAC control law SO(3)/9 using thrusters for $\omega_d = [0.2 \ -0.5 \ 0.3]^T$ rad/sec. (a) Eigenaxis attitude error, (b) angular velocity components, (c) torque inputs, and (d) torque input norm. The spacecraft is initially at rest with $R = I$ and $R_d(0) = I$.

The SO(3)/3 and SO(3)/9 EBAC control laws are able to reject gravity gradient disturbances, as shown in Figure 22 and Figure 23.

Figures 24 and 25 show the closed loop performance of the SO(3)/3 and SO(3)/9 controllers maintaining a fixed inertial pointing. Both controllers are able to follow the command in the presence of a gravity gradient disturbance.

B. EBAC Examples Using Reaction Wheels

Consider the maneuver presented in Section V.C in the presence of an unknown constant nonzero disturbance torque $\tau_{\text{dist}} = [0.7 \ -0.3 \ 0]^T$ N-m. The EBAC controller (76) is used in place of the FGAC controller (40) since (40) lacks an integrator and thus has a constant steady-state error bias due to the persistent disturbance. The parameters of the controller (76) are chosen to be $K_1 = I_3$, $A = \text{diag}(1, 2, 3)$, $\gamma = \eta = 1$, $D = I_3$, and $Q = I_6$.

Figures 26(a)-(f) show, respectively, the attitude error, angular velocity components,

(a)

(b)

(c)

(d)
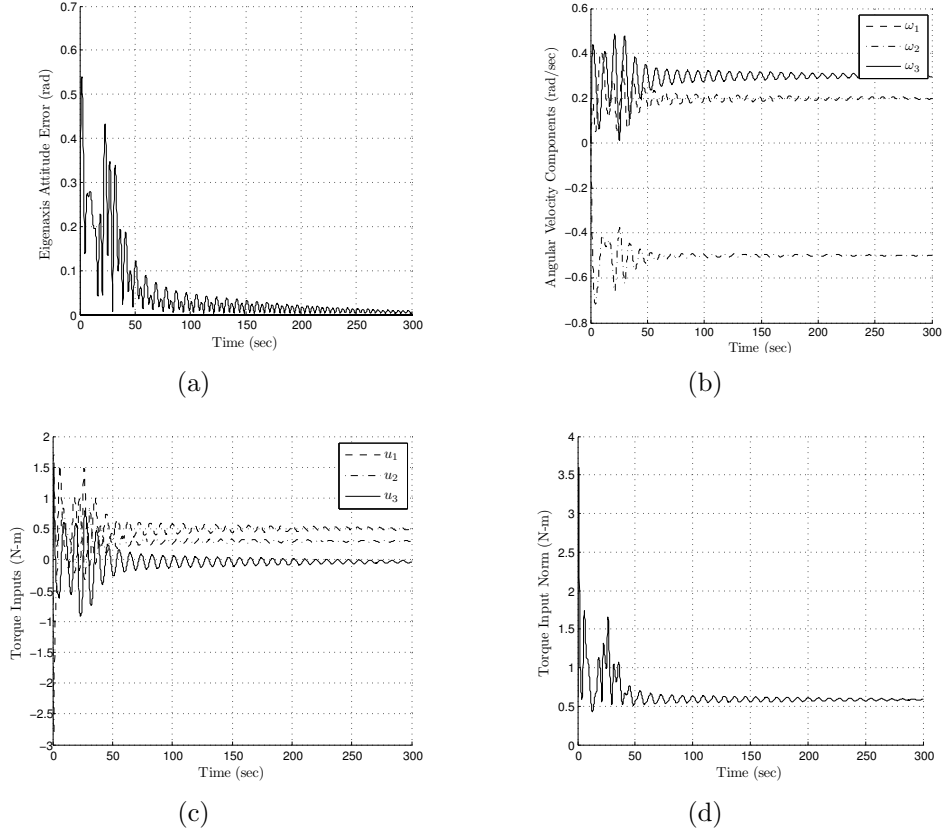
Figure 21. R2S maneuver for the EBAC control law SO(3)/9 using thrusters for $\omega_d = [0.2 \ -0.5 \ 0.3]^T$ rad/sec in the presence of a constant disturbance torque $d = [0 \ 0 \ 0.2]^T$ N-m. (a) Eigenaxis attitude error, (b) angular velocity components, (c) torque inputs, and (d) torque input norm. The spacecraft is initially at rest with $R = I$ and $R_d(0) = I$. The controller is able to reject the disturbance and follow the spin command.

relative-angular-velocity components of the wheels, angular momentum, disturbance-estimate errors, and inertia-estimate errors. The spacecraft attitude and angular velocity components reach the commanded values in about 50 sec. Figure 26(c) indicates that the reaction-wheel rotational speed grows unbounded. Figure 26(d) shows that the total angular momentum of the spacecraft increases consistently with the constant disturbance torque acting on the spacecraft.

Consider, now, a spin maneuver with the spacecraft initially at rest and $R(0) = I_3$. The desired attitude is $R_d(0) = I_3$, and the commanded angular velocity is $\omega_d = [0.5 \ -0.5 \ -0.3]^T$ rad/sec. We assume that no disturbance is present. Figures 27(a)-(e) show, respectively, the attitude error, angular-velocity components, relative-angular-velocity components of the wheels, angular momentum, and inertia-estimate errors. For this maneuver, the spin command consists of a specified time history of rotation about a specified body axis aligned in a specified inertial direction. The controller achieves the commanded motion within about 100 sec.

361
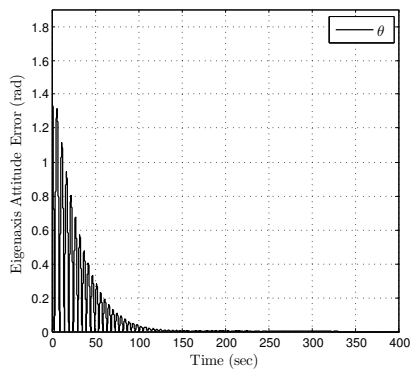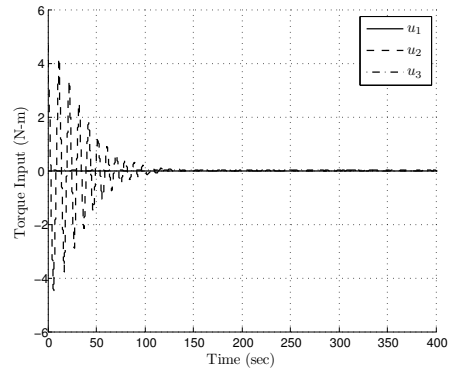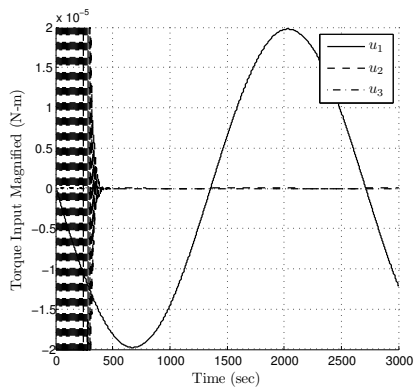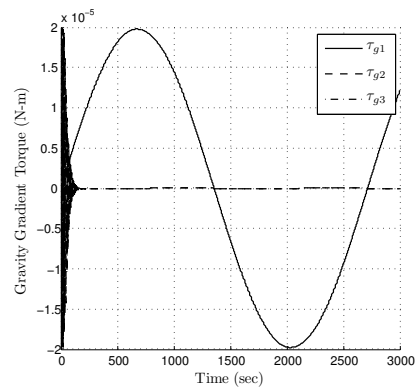
Figure 22. Gravity gradient disturbance rejection for the FGAC control law SO(3)/3 using thrusters. (a) Eigenaxis attitude error, (b) torque input, (c) torque input (magnified), and (d) disturbance torque. The maneuver is a 90-deg rotation about the body-fixed direction $[0\ 1\ 0]^{\mathrm{T}}$. The spacecraft is stabilized, and the disturbance torque is rejected.
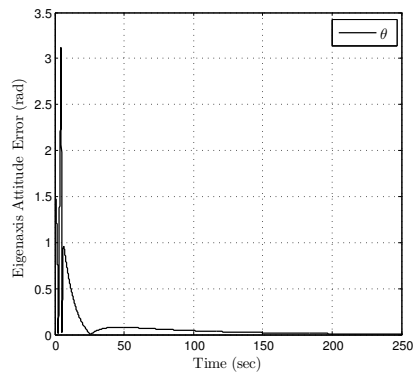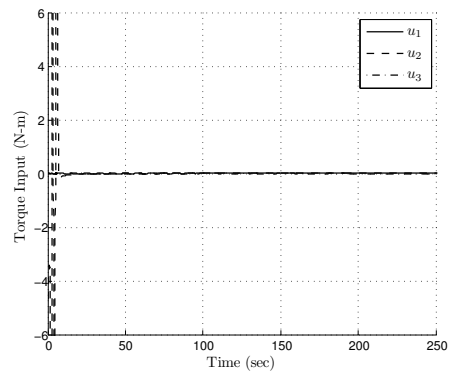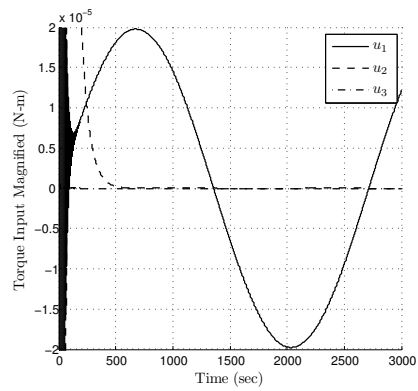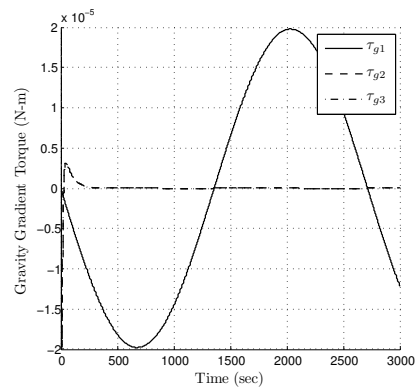
Figure 23. Gravity gradient disturbance rejection for the EBAC control law SO(3)/9 using thrusters. (a) Eigenaxis attitude error, (b) torque input, (c) torque input (magnified), and (d) disturbance torque. The maneuver is a 90-deg rotation about the body-fixed direction $[0\ 1\ 0]^{\mathrm{T}}$. The spacecraft is stabilized, and the disturbance torque is rejected.
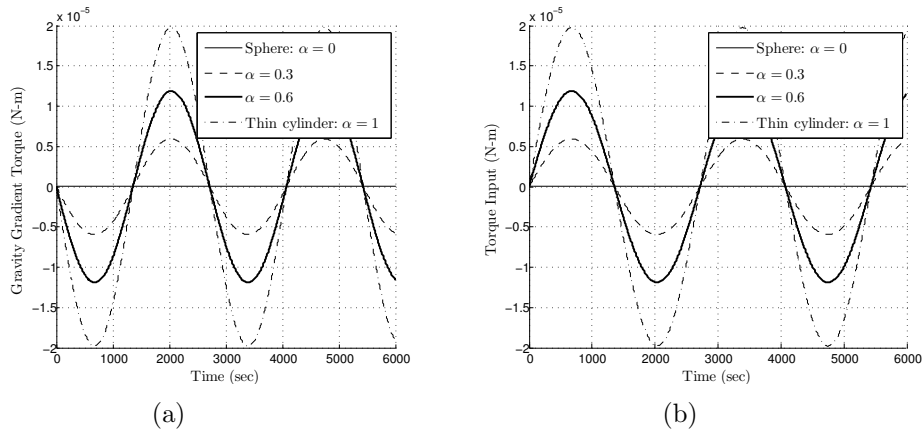
Figure 24. Gravity gradient disturbance for the FGAC control law SO(3)/3 using thrusters. (a) Disturbance torque, and (b) torque input. The desired motion is an equatorial orbital movement with fixed inertial pointing given by $R_d = R(0) = I$. Inertial frame pointing is achieved despite the presence of an attitude-dependent sinusoidal disturbance due to gravity gradients.
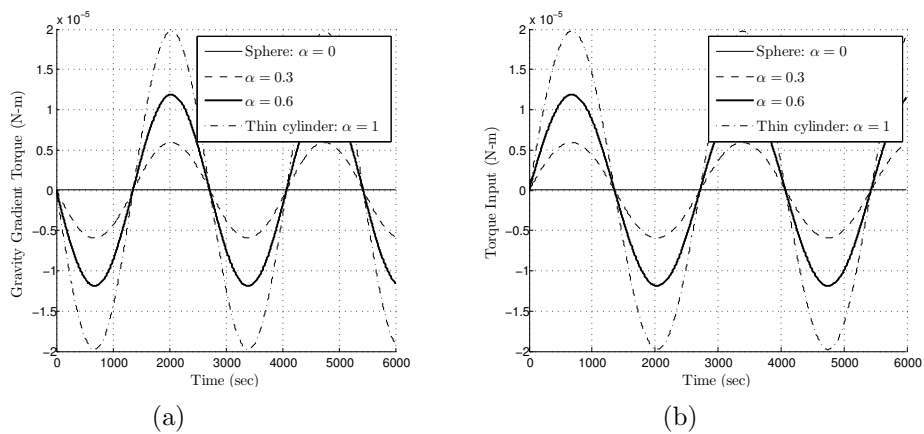
Figure 25. Gravity gradient disturbance for the EBAC control law SO(3)/9 using thrusters. (a) Disturbance torque, and (b) torque input. The desired motion is an equatorial orbital movement with fixed inertial pointing given by $R_d = R(0) = I$. Inertial frame pointing is achieved despite the presence of an attitude-dependent sinusoidal disturbance due to gravity gradients.
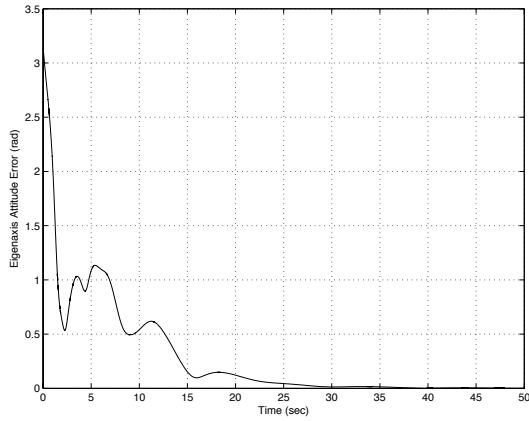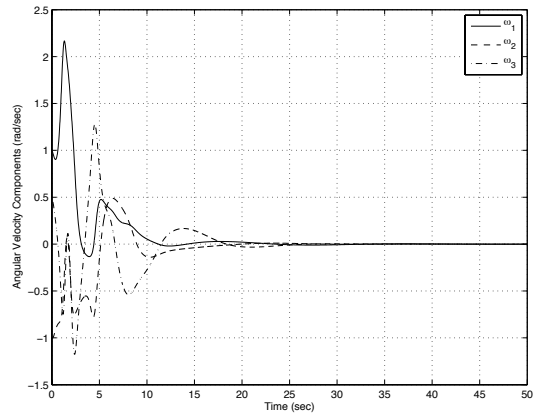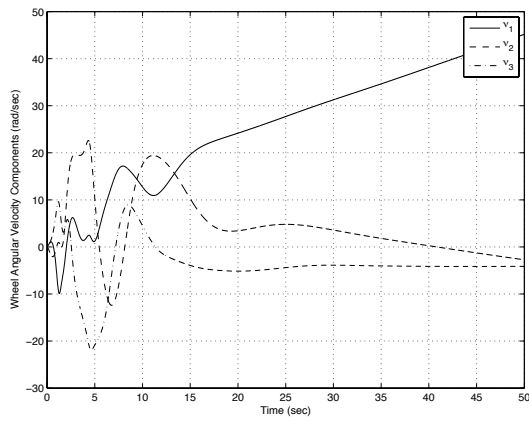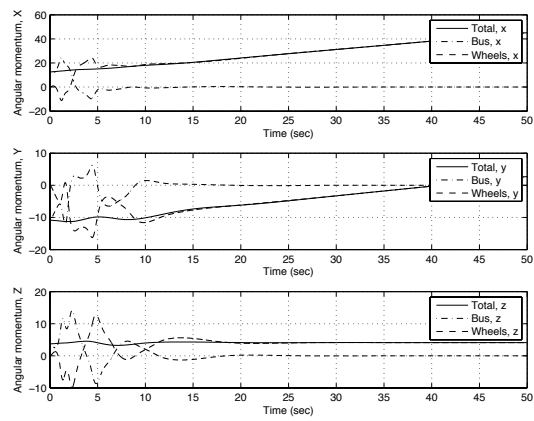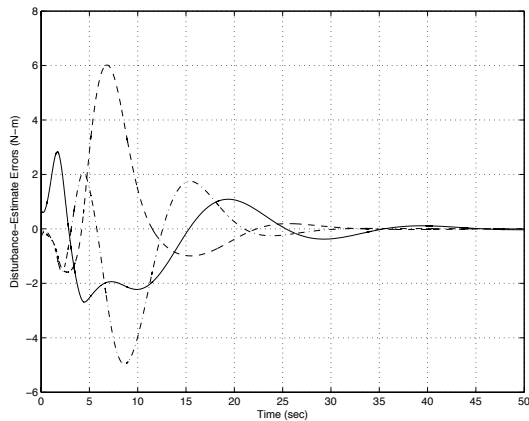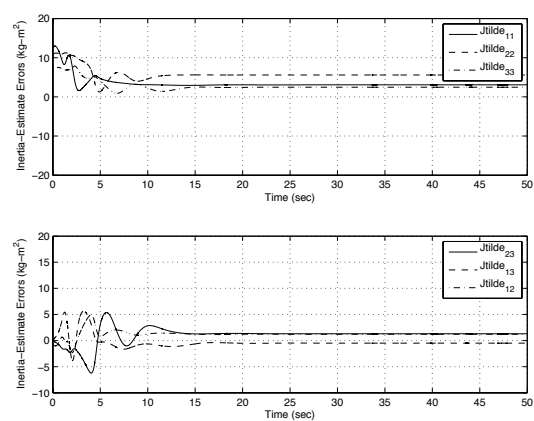
Figure 26. **M2R maneuver for the EBAC control law (76) using reaction wheels with the unknown constant disturbance torque** $\tau_{\text{dist}} = [0.7 \ -0.3 \ 0]^{\text{T}}$ **N-m. (a) Eigenaxis attitude error, (b) spacecraft angular velocity components, (c) wheel angular velocity components, (d) spacecraft angular momentum relative to its center of mass with respect to the inertial frame resolved in the inertial frame, (e) disturbance estimate errors, and (f) inertia estimate errors. The spin rate of the reaction wheels grows unbounded, and the total angular momentum of the spacecraft is not conserved due to the constant disturbance torque.**

365
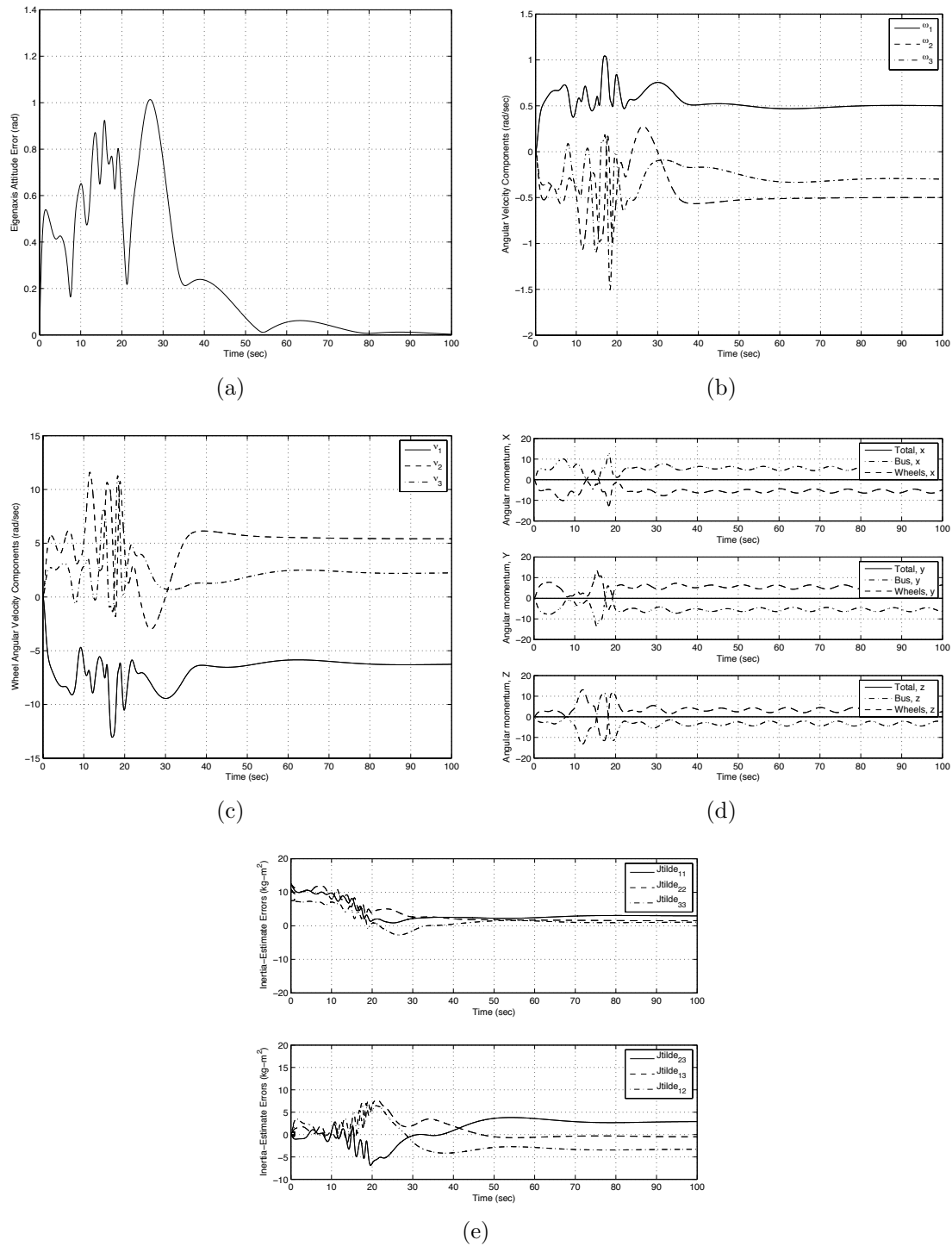
Figure 27. **M2S maneuver for the EBAC control law (76) using reaction wheels. The desired attitude is $R_\mathrm{d}(0) = I_3$, and the commanded angular velocity is $\omega_\mathrm{d} = [0.5 \ -0.5 \ -0.3]^\mathrm{T}$ rad/sec. (a) Eigenaxis attitude error, (b) spacecraft angular velocity components, (c) wheel angular velocity components, (d) spacecraft angular momentum relative to its center of mass with respect to the inertial frame resolved in the inertial frame, and (e) inertia estimate errors. No disturbance is present.**

C.   EBAC Examples Using CMG's

Consider the maneuver presented in Section V.D in the presence of an unknown constant nonzero disturbance torque $\tau_{\text{dist}} = [0.35 \; -0.015 \; 0]^{\text{T}}$ N-m. Note that the EBAC controller (78) is used in place of the FGAC controller (40) since (40) lacks an integrator and thus has a constant steady-state error bias due to the persistent disturbance. The parameters of the controller (78) are chosen to be $K_1 = I_3$, $A = \text{diag}(1, 2, 3)$, $D = I_3$, and $Q = I_6$.

Figures 28(a)-(e) show, respectively, the attitude error, angular-velocity components, gimbal angles, inertia-estimate errors, and singular values of B. The spacecraft attitude and angular velocity components reach the commanded values in about 35 sec. Figure 28(c) indicates that the CMG gimbal angles grow unbounded.

Next, we consider a spin maneuver with the spacecraft initially at rest and $R(0) = I_3$. The desired attitude is determined by $R_{\text{d}}(0) = I_3$, and the commanded angular velocity is $\omega_{\text{d}} = [0.005 \; -0.005 \; -0.003]^{\text{T}}$ rad/sec. We assume that no disturbance is present. Figures 29(a)-(e) show, respectively, the attitude error, angular-velocity components, gimbal angles, inertia-estimate errors, and singular values of B. For this maneuver, the spin command consists of a specified time history of rotation about a specified body axis aligned in a specified inertial direction. The controller achieves the commanded motion within about 20 sec.
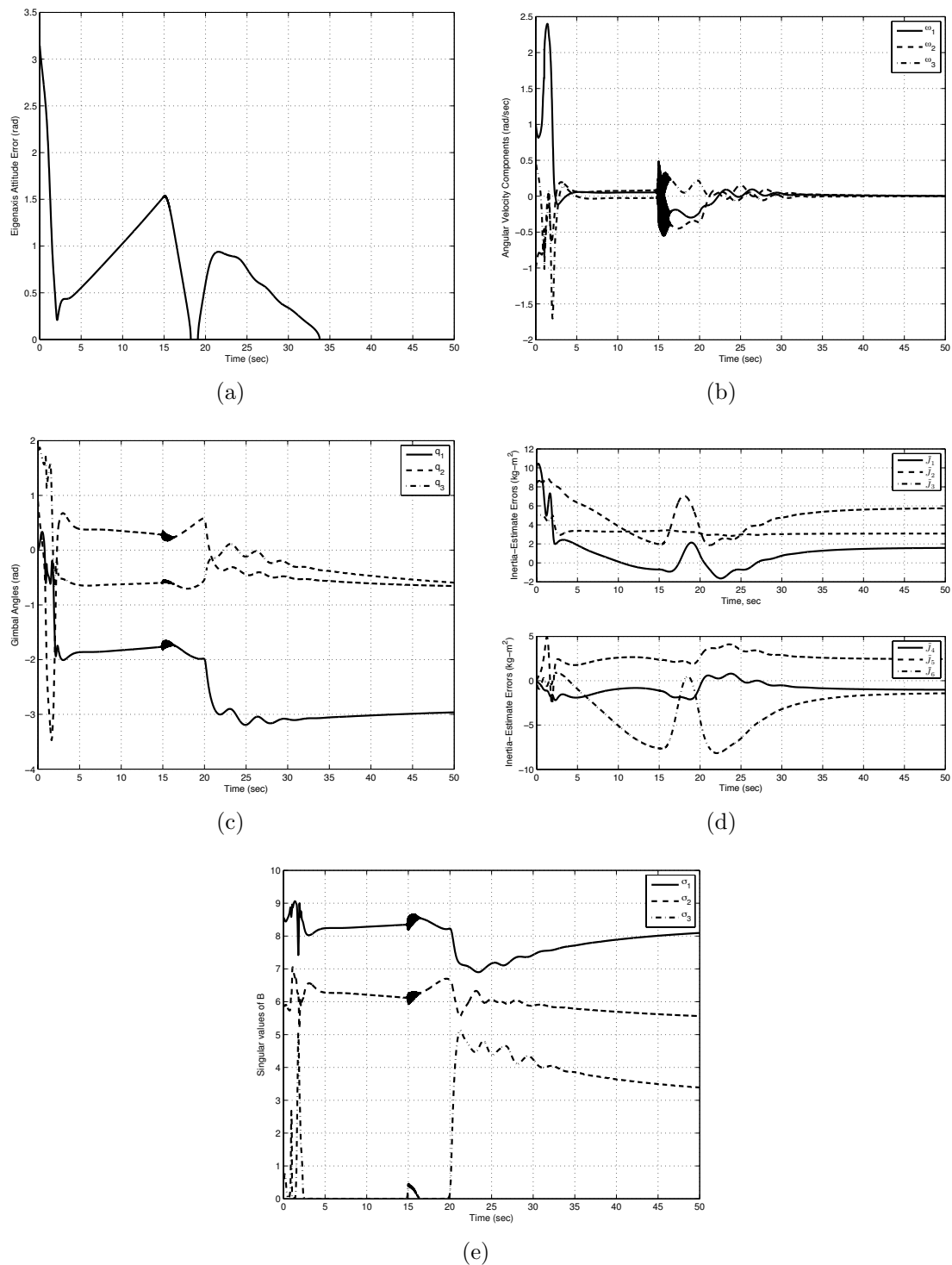
Figure 28. M2R maneuver for the EBAC control law (**78**) using CMG's with the unknown constant disturbance torque $\tau_{\text{dist}} = [0.35 \; -0.015 \; 0]^{\text{T}}$ **N-m. (a) Eigenaxis attitude error, (b) spacecraft angular velocity components, (c) gimbal angles, (d) inertia estimate errors, and (e) singular values of** B**.**
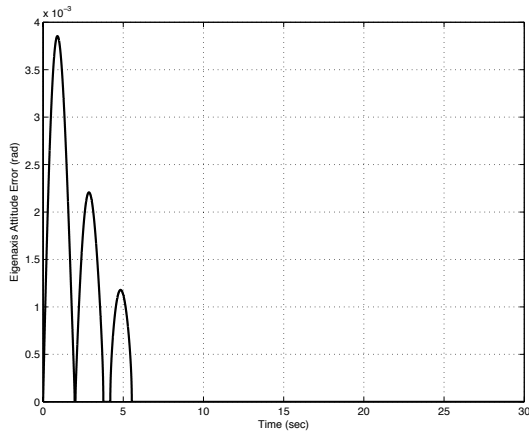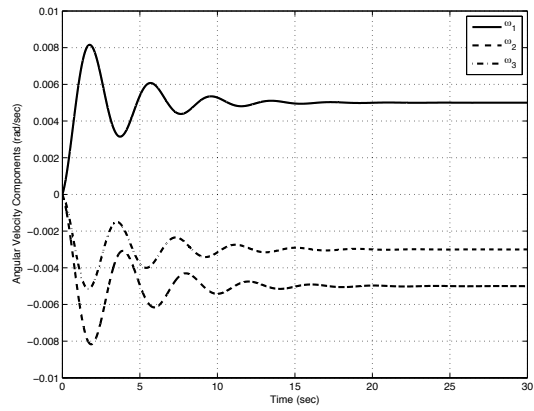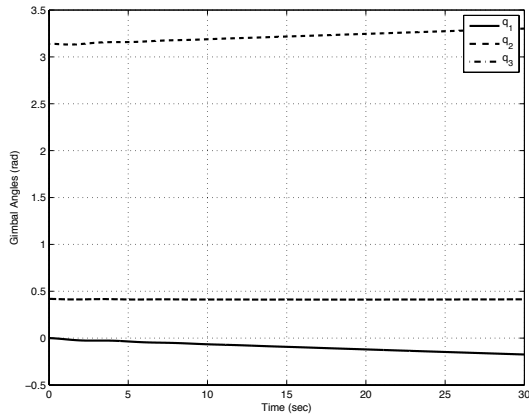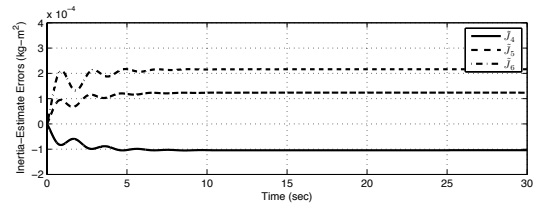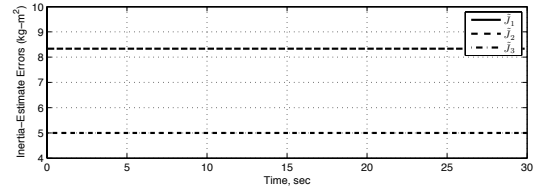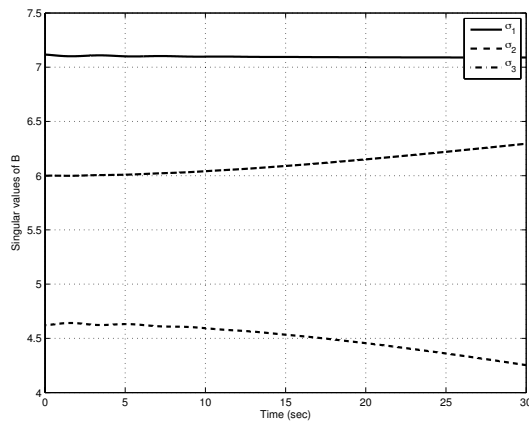
Figure 29. **M2S maneuver for the EBAC control law (78) using CMG's. The desired attitude is determined by $R_{\mathrm{d}}(0) = I_3$, and the commanded angular velocity is $\omega_{\mathrm{d}} = [0.005 \quad -0.005 \quad -0.003]^{\mathrm{T}}$ rad/sec. (a) Eigenaxis attitude error, (b) spacecraft angular velocity components, (c) gimbal angles, (d) inertia estimate errors, and (e) singular values of B. No disturbance is present.**

VIII.   Retrospective Cost Attitude Control (RCAC)

In this section we provide a brief description of the retrospective cost adaptive control technique. This technique is based on discrete-time adaptive control algorithms developed for linear systems. In particular, in [31] a Lyapunov-function-based proof of stability and convergence is provided for stabilization, command following, and disturbance-rejection problems. This result applies to minimum-phase linear systems that are SISO or MIMO and possibly open-loop unstable, where the commands and disturbances are generated by a Lyapunov-stable exogenous system (that is, the command and disturbance are sums of sinusoids and steps) [58]. Within this class of systems, the adaptive controller of [31] requires a bound on the first nonzero Markov parameter as well as bounds on the order of the plant dynamics and exosystem dynamics.

A restrictive assumption in [31], however, as in many other adaptive control approaches (especially those that invoke positive realness or almost positive realness), is the restriction to minimum-phase systems. The issue of nonminimum-phase (NMP) zeros can be circumvented by implementing full-state sensing, which implies that the plant has no zeros. However, in many applications, full-state feedback corresponds to unrealistic sensing requirements. To address this case, retrospective cost adaptive control has been developed for nonminimum-phase systems. The earliest version of this algorithm can be traced to [59], with subsequent development in [34, 60]. As shown in [34], no knowledge of the poles of the system is needed; no positive real or almost positive real assumptions need to be satisfied; no constraint on the allowable relative degree must be satisfied; no prior parameter set is needed; persistent excitation is not needed; the commands and disturbances may be uncertain in terms of amplitude, phase, and spectrum; and no matching conditions are required on either the plant uncertainty or the exogenous disturbances. In addition, for plants that are Lyapunov stable, precise knowledge of the nonminimum-phase zeros is not needed [35, 36, 61, 62].

Retrospective cost adaptive control is a direct-digital approach, which means that retrospective cost adaptive control is a discrete-time control law that can be used for sampled-data implementation without first producing a continuous-time control law. Direct digital control does not require controller digitization, and thus facilitates embedded code generation. For identification-based modeling, the required discrete-time modeling information can be obtained from the sampled data. In particular, RCAC can use knowledge of Markov parameters, which depend on the sampled discrete-time dynamics at the prescribed sample rate. Least-squares methods [63] can then be used to estimate the required discrete-time modeling information. Finally, retrospective cost adaptive control does not require signal derivatives, either directly or as filtered versions.

Consider the MIMO discrete-time system

$$x(k+1) = Ax(k) + Bu(k), \tag{83}$$
$$y_0(k) = E_1 x(k), \tag{84}$$
$$z(k) = y_0(k) - E_0 r(k), \tag{85}$$

where $x(k) \in \mathbb{R}^{l_x}$, $y_0(k) \in \mathbb{R}^{l_y}$, $z(k) \in \mathbb{R}^{l_z}$, $u(k) \in \mathbb{R}^{l_u}$, $r(k) \in \mathbb{R}^{l_w}$, and $k \geq 0$.

A. Retrospective Cost

For $i \geq 1$, define the Markov parameter of G_{zu} given by

$$H_i \triangleq E_1 A^{i-1} B. \tag{86}$$

For example, $H_1 = E_1 B$ and $H_2 = E_1 A B$. Let n be a positive integer. Then, for all $k \geq n$,

$$x(k) = A^n x(k-n) + \sum_{i=1}^{n} A^{i-1} B u(k-i) \tag{87}$$

thus

$$z(k) = E_1 A^n x(k-n) + \bar{H} \bar{U}(k-1) - E_0 r(k), \tag{88}$$

where

$$\bar{H} \triangleq \begin{bmatrix} H_1 & \cdots & H_n \end{bmatrix} \in \mathbb{R}^{l_z \times n l_u}$$

and

$$\bar{U}(k-1) \triangleq \begin{bmatrix} u(k-1) \\ \vdots \\ u(k-n) \end{bmatrix} \in \mathbb{R}^{n l_u}.$$

Next, assume we know $l_{\mathcal{H}}$ Markov parameters, rearrange the columns of $\bar{H}$ and the entries of $\bar{U}(k-1)$ then partition the resulting matrix and vector so that

$$\bar{H} \bar{U}(k-1) = \mathcal{H}' U'(k-1) + \mathcal{H} U(k-1). \tag{89}$$

where $U \in \mathbb{R}^{l_{\mathcal{H}} l_u}$ and $U' \in \mathbb{R}^{(n-l_h) l_u}$. Furthermore, $\mathcal{H} \in \mathbb{R}^{l_z \times l_{\mathcal{H}} l_u}$ and $\mathcal{H}' \in \mathbb{R}^{l_z \times l_u (n-l_{\mathcal{H}})}$ are the known and unknown Markov parameters respectively. For example, if $\bar{H} = \begin{bmatrix} H_1 & H_2 & H_3 \end{bmatrix}$, we can divide it into $\mathcal{H}' = \begin{bmatrix} H_1 & H_3 \end{bmatrix}$ with $U'(k-1) = \begin{bmatrix} u(k-1) \\ u(k-3) \end{bmatrix}$ then $\mathcal{H} = H_2$ with the corresponding $U = u(k-2)$. We can rewrite (88) as

$$z(k) = \mathcal{S}(k) + \mathcal{H} U(k-1), \tag{90}$$

where

$$\mathcal{S}(k) \triangleq E_1 A^n x(k-n) - E_0 r(k) + \mathcal{H}' U'(k-1) \tag{91}$$

collects all the unknown parameters of the system.

Let s be a positive integer, then for $j = 1, \ldots, s$, we add a delay k_j in (90) so that $0 \le k_1 \le k_2 \le \cdots \le k_s$. The delayed performance is

$$z(k - k_j) = \mathcal{S}_j(k - k_j) + \mathcal{H}_j U_j(k - k_j - 1). \tag{92}$$

where

$$\mathcal{S}_j(k - k_j) \triangleq E_1 A^n x(k - k_j - n) - E_0 r(k - k_j) + \mathcal{H}'_j U'_j(k - k_j - 1), \tag{93}$$

and (89) becomes

$$\bar{H} \bar{U}(k - k_j - 1) = \mathcal{H}'_j U'_j(k - k_j - 1) + \mathcal{H}_j U_j(k - k_j - 1). \tag{94}$$

We stack $z(k - k_1), \ldots, z(k - k_s)$, and define the *extended performance*

$$Z(k) \triangleq \begin{bmatrix} z(k - k_1) \\ \vdots \\ z(k - k_s) \end{bmatrix} \in \mathbb{R}^{sl_z}. \tag{95}$$

Therefore,

$$Z(k) \triangleq \tilde{\mathcal{S}}(k) + \tilde{\mathcal{H}} \tilde{U}(k - 1), \tag{96}$$

where

$$\tilde{\mathcal{S}}(k) \triangleq \begin{bmatrix} \mathcal{S}_1(k - k_1) \\ \vdots \\ \mathcal{S}_s(k - k_s) \end{bmatrix} \in \mathbb{R}^{sl_z}, \tag{97}$$

and $\tilde{U}(k - 1)$ has the form

$$\tilde{U}(k - 1) \triangleq \begin{bmatrix} u(k - q_1) \\ \vdots \\ u(k - q_g) \end{bmatrix} \in \mathbb{R}^{gl_u}, \tag{98}$$

where $k_1 \le q_1 < q_2 < \cdots < q_g \le k_s + n$. The vector $\tilde{U}(k - 1)$ is formed by stacking $U_1(k - k_1 - 1), \ldots, U_s(k - k_s - 1)$ and removing copies of repeated components, and $\tilde{\mathcal{H}} \in \mathbb{R}^{sl_z \times gl_u}$ is constructed according to the structure of $\tilde{U}(k - 1)$.

We also define the *retrospective performance*,

$$\hat{z}(k - k_j) \triangleq \mathcal{S}_j(k - k_j) + \mathcal{H}_j \hat{U}_j(k - k_j - 1), \tag{99}$$

where the past controls $U_j(k - k_j - 1)$ in (92) are replaced by the retrospective controls

$\hat{U}_j(k - k_j - 1)$, which are computed in (108) below. As in (95), we define the *extended retrospective performance*

$$\hat{Z}(k) \triangleq \begin{bmatrix} \hat{z}(k - k_1) \\ \vdots \\ \hat{z}(k - k_s) \end{bmatrix} \in \mathbb{R}^{sl_z}, \tag{100}$$

thus

$$\hat{Z}(k) = \tilde{\mathbb{S}}(k) + \tilde{\mathcal{H}}\hat{\tilde{U}}(k - 1), \tag{101}$$

where the components of $\hat{\tilde{U}}(k-1) \in \mathbb{R}^{l_{\tilde{U}}}$ are the components of $\hat{U}_1(k-k_1-1), \ldots, \hat{U}_s(k-k_s-1)$ ordered in the same way as the components of $\tilde{U}(k-1)$. Subtracting the extended performance in (96) from the extended retrospective performance in (101) yields

$$\hat{Z}(k) = Z(k) - \tilde{\mathcal{H}}\tilde{U}(k - 1) + \tilde{\mathcal{H}}\hat{\tilde{U}}(k - 1). \tag{102}$$

Thus, we define the *retrospective cost function*

$$J(\hat{\tilde{U}}(k - 1), k) \triangleq \hat{Z}^{\mathrm{T}}(k)R(k)\hat{Z}(k), \tag{103}$$

where $R(k) \in \mathbb{R}^{l_z s \times l_z s}$ is a positive-definite performance weighting.

The goal is to determine the retrospective controls $\hat{\tilde{U}}(k - 1)$ that minimize the retrospective performance $\hat{Z}(k)$. These retrospectively optimized control values $\hat{\tilde{U}}(k-1)$ are then used to update the controller. To this end we solve the optimization problem in (103).

Expanding (103) with (102) yields

$$J(\hat{\tilde{U}}(k - 1), k) = \hat{\tilde{U}}(k - 1)^{\mathrm{T}}\mathcal{A}(k)\hat{\tilde{U}}(k - 1) + \hat{\tilde{U}}^{\mathrm{T}}(k - 1)\mathcal{B}^{\mathrm{T}}(k) + \mathcal{C}(k), \tag{104}$$

where

$$\mathcal{A}(k) \triangleq \tilde{\mathcal{H}}^{\mathrm{T}}R(k)\tilde{\mathcal{H}}, \tag{105}$$

$$\mathcal{B}(k) \triangleq 2\tilde{\mathcal{H}}^{\mathrm{T}}R(k)[Z(k) - \tilde{\mathcal{H}}\tilde{U}(k - 1)], \tag{106}$$

$$\mathcal{C}(k) \triangleq Z^{\mathrm{T}}(k)R(k)Z(k) - 2Z^{\mathrm{T}}(k)R(k)\tilde{\mathcal{H}}\tilde{U}(k - 1) + \tilde{U}^{\mathrm{T}}(k - 1)\tilde{\mathcal{H}}^{\mathrm{T}}R(k)\tilde{\mathcal{H}}\tilde{U}(k - 1). \tag{107}$$

Given a full column rank $\tilde{\mathcal{H}}$, $\mathcal{A}(k)$ is positive definite and $J(\hat{\tilde{U}}(k - 1), k)$ has a unique global minimizer which is the optimized retrospective control

$$\hat{\tilde{U}}(k - 1) = -\frac{1}{2}\mathcal{A}^{-1}(k)\mathcal{B}(k). \tag{108}$$

B.   Controller Construction

We design a strictly proper time-series controller of order n_c given by

$$u(k) = \sum_{i=1}^{n_c} M_i(k)u(k-i) + \sum_{i=1}^{n_c} N_i(k)z(k-i), \tag{109}$$

where, for all $i = 1, \ldots, n_c$, $M_i(k) \in \mathbb{R}^{l_u \times l_u}$ and $N_i(k) \in \mathbb{R}^{l_u \times l_z}$. The control (109) can be expressed as

$$u(k) = \theta(k)\phi(k-1), \tag{110}$$

where

$$\theta(k) \triangleq [M_1(k) \ \cdots \ M_{n_c}(k) \ N_1(k) \ \cdots \ N_{n_c}(k)] \in \mathbb{R}^{l_u \times n_c(l_u + l_z)} \tag{111}$$

and

$$\phi(k-1) \triangleq \begin{bmatrix} u(k-1) \\ \vdots \\ u(k-n_c) \\ z(k-1) \\ \vdots \\ z(k-n_c) \end{bmatrix} \in \mathbb{R}^{n_c(l_u + l_z)}. \tag{112}$$

C.   Recursive Least Squares Update of $\theta(k)$

Define the cumulative cost function

$$J_{\mathrm{R}}(\theta(k)) \triangleq \sum_{i=q_g+1}^{k} \lambda^{k-i} \|\phi^{\mathrm{T}}(i - q_g - 1)\theta^{\mathrm{T}}(k) - \hat{u}^{\mathrm{T}}(i - q_g)\|^2$$
$$+ \lambda^k(\theta(k) - \theta(0))P^{-1}(0)(\theta(k) - \theta(0))^{\mathrm{T}}, \tag{113}$$

where $\|\cdot\|$ is the Euclidean norm and, for some $\varepsilon \in (0,1)$, $\lambda(k) \in (\varepsilon, 1]$ is the forgetting factor, and $P(0) \in \mathbb{R}^{n_c(l_u+l_z) \times n_c(l_u+l_z)}$ is the initial covariance matrix. Minimizing (113) yields

$$\theta^{\mathrm{T}}(k) \triangleq \theta^{\mathrm{T}}(k-1) + \beta(k)P(k-1)\phi(k - q_g - 1)$$
$$\cdot [\phi^{\mathrm{T}}(k - q_g - 1)P(k-1)\phi(k - q_g - 1) + \lambda(k)]^{-1}[\theta(k-1)\phi(k - q_g - 1) - \hat{u}(k - q_g)]^{\mathrm{T}}, \tag{114}$$

where $\beta(k)$ is a switch on the control such that

$$\beta(k) = \begin{cases} 0 & k < k_{\text{on}} \\ 1 & k \geq k_{\text{on}} \end{cases} \tag{115}$$

and k_{on} is the time step at which we wish the controller to start operating.

The error covariance is updated by

$$P(k) \triangleq [1 - \beta(k)]P(k-1) + \beta(k)\lambda^{-1}(k)P(k-1) - \beta(k)\lambda^{-1}(k)P(k-1)\phi(k-q_g-1)$$
$$\cdot [\phi^{\mathrm{T}}(k-q_g-1)P(k-1)\phi(k-q_g-1) + \lambda(k)]^{-1}\phi^{\mathrm{T}}(k-q_g-1)P(k-1). \tag{116}$$

We initialize the error covariance matrix as $P(0) = \gamma I$, where $\gamma > 0$. Furthermore, the updates (114) and (116) are based on the gth component of $\hat{\tilde{U}}(k-1)$. However any or all of the components of $\hat{\tilde{U}}(k-1)$ may be used in the update of $\theta(k)$ and $P(k)$.

D. Performance Variable for Spacecraft Attitude Control

RCAC requires a vector performance variable, and thus the rotation matrix governed by Poisson's equation (2), cannot be used directly. We therefore reformulate the attitude error dynamics by using the vector function of the attitude error matrix presented in [22]. For $i = 1, 2, 3$, let e_i denote the ith column of the 3×3 identity matrix and let $A_{\text{att}} = \text{diag}(a_1, a_2, a_3)$ be a diagonal positive-definite matrix, then

$$z_a \triangleq \sum_{1}^{3} a_i(\tilde{R}^{\mathrm{T}}e_i) \times e_i, \tag{117}$$

is a 3×1 vector measure of attitude error. Note that $z_a = 0$ when $\tilde{R} = I_3$. Thus, we use z_a as the attitude performance variable. We define the angular rate performance as

$$z_\omega \triangleq \omega - \tilde{R}^{\mathrm{T}}\omega_d. \tag{118}$$

The combined performance variable for the attitude control problem is given by

$$z = \begin{bmatrix} z_\omega \\ z_a \end{bmatrix}. \tag{119}$$

Parameter	Description	Value
n_c	Controller order	3
P_0	Initial error covariance used in the RLS update	$100I$
R	Performance weighting to compute the retrospective cost function	I
s	Number of data points used for retrospective cost computation	1
k_s	Delay used to construct the extended performance vector	1
θ_0	Initial controller coefficients	0
$\lambda(k)$	Forgetting factor	1
h	Controller time step	0.1
k_{on}	Number of time steps to wait before applying first control action	81
A_{att}	Weighting on the attitude error matrix $\tilde{R}$ used in z_a	I_3

Table 1. RCAC Parameters.

IX. RCAC Examples

A. M2R Maneuvers Using Thrusters

Let the spacecraft inertia matrix be defined by $J_{\mathrm{sc}} = J_3$. In the absence of disturbances, we consider a M2R maneuver involving an eigenaxis rotation of $40°$ about the body fixed direction $[1\ 1\ 1]^{\mathrm{T}}$ with the spacecraft initially at $R(0) = I_3$

The RCAC parameters used are shown in Table 1. For the M2R problem, we utilize the inertia-free Markov parameter

$$\hat{H}_1 = \begin{bmatrix} hB_{\mathrm{sc}} \\ h^2 B_{\mathrm{sc}} \end{bmatrix}. \tag{120}$$

where h is the controller time step and we assume $B_{\mathrm{sc}} = I_3$. Furthermore, we apply a proportional saturation to the commanded control input by scaling the control vector as

$$u_{\mathrm{sat}} = \begin{cases} u, & u \in \mathcal{B}, \\ \eta u, & u \notin \mathcal{B}, \end{cases} \tag{121}$$

where $\mathcal{B}$ is a boundary defined by the saturation limits and η is the maximum scaling such that $u_{sat} \in \mathcal{B}$, that is,

$$\eta = \max_{\eta \in (0,1]} \{\eta : \eta u \in \mathcal{B}\}. \tag{122}$$

1. Inertia Variations

We use two approaches to examine the effect of inertia variations on the settling M2R time. First we begin with the centroid inertia J_3 and move towards the other inertia types according to

$$J_{\text{sc}} = (1 - \alpha)J_3 + \alpha J_i, \text{ for } i = 1, 2, 4, 5. \tag{123}$$

We vary the weighting α and examine the settling time for the M2R maneuver in Figures 30 and 31.
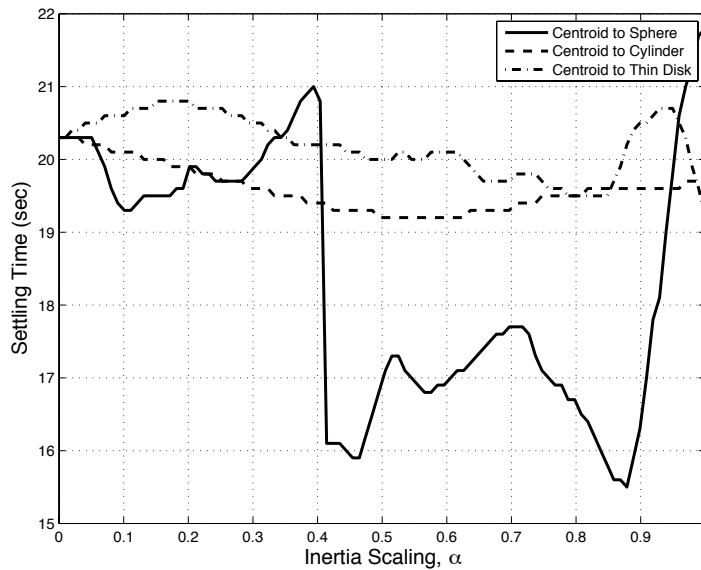
Figure 30. M2R settling time for the RCAC control law using thrusters. The inertia J_{sc} starts at the centroid value J_3 and moves toward the sphere J_1, cylinder J_2, and thin disk J_4 inertias according to (123). The saturation level is set at 1 N-m.

For the second approach we again start with the centroid inertia J_3. We examine the M2R settling time as the actuator and sensor axes are rotated away from the principal axis according to

$$J_{\text{sc}} = R_i(\phi)J_3 R_i(\phi)^{\text{T}}. \tag{124}$$

Where $R_i(\phi) \in \mathbb{R}^{3\times 3}$ for $i = 1, 2, 3$ is the rotation matrix given by Rodrigues' formula

$$\mathcal{R}(\phi, e_i) = \cos(\phi)I_3 + (1 - \cos(\phi))e_i e_i^{\text{T}} + \sin(\theta)e_i^{\times}, \tag{125}$$

where ϕ is the misalignment angle and e_i is the ith column of the 3×3 identity matrix. We examine the settling time as a function of θ in Figure 32.

377
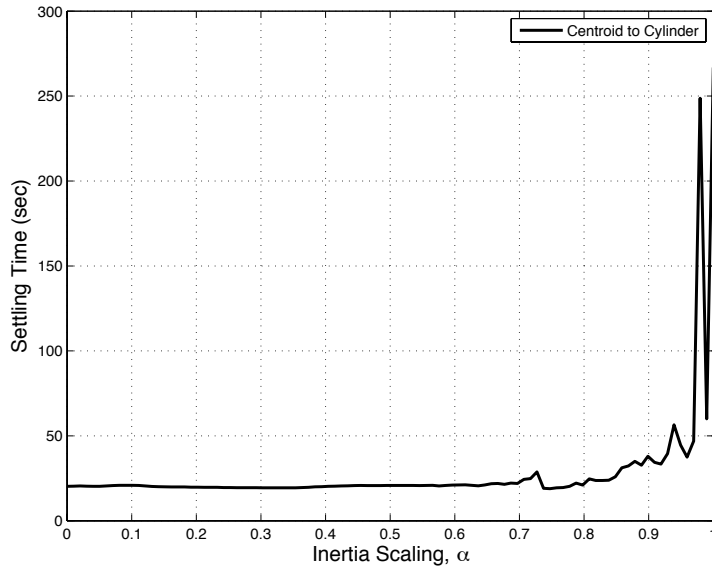
Figure 31. M2R settling time for the RCAC control law using thrusters. The inertia $J_{\rm sc}$ starts at the centroid value J_3 and moves toward the thin cylinder inertia J_5 according to (123). The saturation level is set at 1 N-m.

2. Saturation Level

We examine the M2R settling time for RCAC under varying levels of saturation. We define the boundary $\mathcal{B}$ in (121) by setting saturation limits for each axis

$$u_{\rm lim} = u_{\rm max} \begin{bmatrix} 1 & 1 & 1 \end{bmatrix}^{\rm T} \text{ N-m.} \tag{126}$$

We let $J_{\rm sc} = J_3$ and vary $u_{\rm max}$. Figure 33 shows the settling time as a function of saturation level.

3. On-Off Thrusters

We introduce an input nonlinearity in the form of on-off thrusters. The applied control torque to the spacecraft is

$$u = \text{sign}(u_{\rm cmd})u_{\rm on} \tag{127}$$

where $u_{\rm on}$ is a positive scalar and $u_{\rm cmd}$ is the commanded torque computed using RCAC. We examine the effect of the on-off nonlinearity on the M2R settling time. We let $J_{\rm sc} = J_3$ and vary the thruster torque $u_{\rm on}$. Figure 34 shows that as $u_{\rm on}$ increases the spacecraft takes more time to complete the maneuver.

378
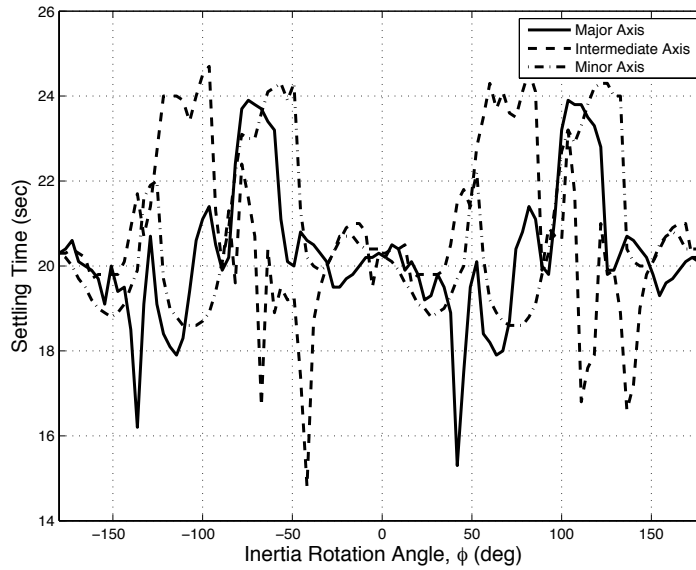
Figure 32. M2R settling time for the RCAC control law using thrusters. The inertia J_{sc} starts at the centroid value J_3 and is rotated about each principal axis by ϕ. The saturation level is set at 1 N-m on each axis.

4. Constant Disturbance

We examine the effect of disturbances on the M2R settling time. We let $J_{sc} = J_3$ and consider a constant unknown disturbance z_{dist} about each principal axis of the form

$$z_{dist} = \beta e_i, \tag{128}$$

where e_i is the ith column of the 3×3 identity matrix. We vary the disturbance level β and examine its effect on M2R settling time. Figure 35 shows the settling time as a function of the disturbance level β.

B. M2S Maneuvers Using Thrusters

For the M2S maneuver, we again take the spacecraft inertia to be $J_{sc} = J_3$ and let the spacecraft be initially at rest so that $R(0) = I$. We test four maneuvers. First, we command the spacecraft to spin about each of the principal axes so that

$$\omega_d = 0.1 e_i \text{ rad/sec, for } i = 1, 2, 3. \tag{129}$$
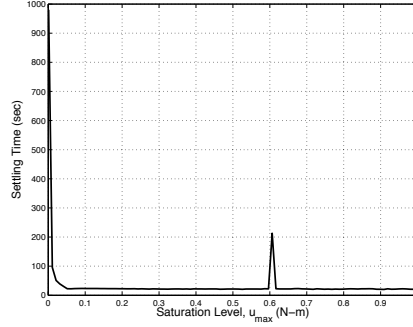
Figure 33. M2R settling time for the RCAC control law using thrusters as a function of saturation level u_{max} for RCAC using thrusters.
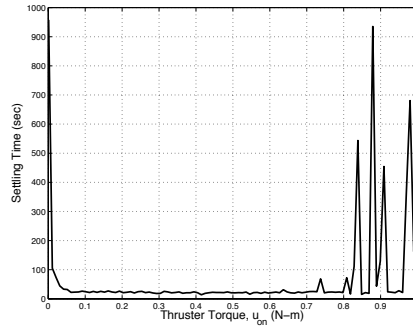
Figure 34. M2R settling time for the RCAC control law using on-off thrusters as a function of the thrust level u_{on}.

where e_i is the ith column of I_3. For the fourth test we command the spacecraft to spin about the non-principal body-fixed axis

$$\omega_{\mathrm{d}} = \frac{0.1}{\sqrt{3}} \begin{bmatrix} 1 & 1 & 1 \end{bmatrix}^{\mathrm{T}} \mathrm{rad/sec}. \tag{130}$$

We command a 40° eigenaxis rotation about the vector $[1\ 1\ 1]^{\mathrm{T}}$. However, the desired attitude evolves according to $\dot{R}_{\mathrm{d}} = R_{\mathrm{d}}\omega^{\times}$. Figure 36 shows the closed-loop response for the M2S maneuver.

C. M2R Maneuvers Using Reaction Wheels

Consider the rigid body defined by the inertia tensor $J_{\mathrm{sc}} = J_3$ with three orthogonal reaction wheels. The moment of inertia about each wheel's rotational axis is $J_{W_i} = 0.1$ kg/m² and the spin axis for each wheel resolved in the wheel's frame is $e_{W_i} = [1\ 0\ 0]^{\mathrm{T}}$ for $i = 1, 2, 3$. Furthermore, the wheels are aligned with the body axes of the spacecraft such that each wheel's spin axis is parallel to the principal moments of inertia of the spacecraft so that the orientation matrices from the wheel frame W_i to the spacecraft
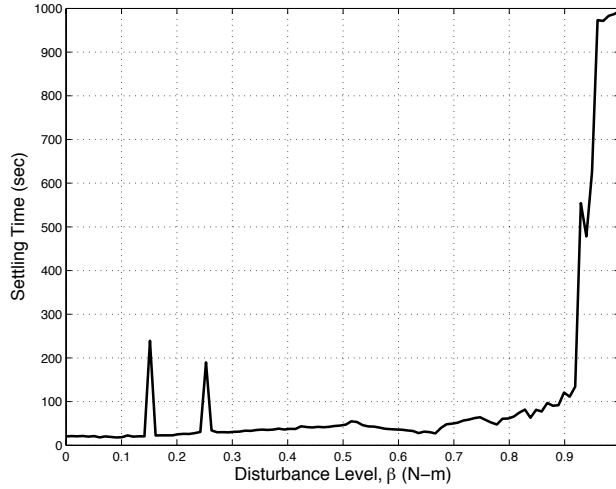
Figure 35. M2R closed-loop performance for the RCAC control law using thrusters. Settling time as a function of the constant disturbance magnitude β about each principal axis. The number of previous time steps in the retrospective cost is set to $s = 1$. The saturation level is set at 1 N-m, which is sufficient to reject the disturbance for all $\beta \in [0, 1]$.

body frame are

$$\mathcal{O}_{B/W_i} = I_3, \quad i = 1, 2, 3. \tag{131}$$

Using these matrices in the spacecraft dynamics in (19) and the reaction wheel dynamics in (20) result in the input matrix

$$B_{\mathrm{sc}} = -\mathrm{diag}(J_{W_1}, J_{W_2}, J_{W_3}). \tag{132}$$

We consider a M2R maneuver involving an eigenaxis rotation of $40°$ about the body fixed direction $[1\ 1\ 1]^{\mathrm{T}}$ with the spacecraft initially at $R(0) = I_3$ and no disturbances. The reaction wheels are initially at rest so that

$$\nu_i(0) = \begin{bmatrix} 0 & 0 & 0 \end{bmatrix}^{\mathrm{T}} \mathrm{rad/sec}, \quad i = 1, 2, 3. \tag{133}$$

For the RCAC parameters, we use Table 1 and set $s = 1$. We use the inertia-free Markov parameter

$$\hat{H}_1 = -\begin{bmatrix} h\hat{B}_{\mathrm{sc}} \\ h^2\hat{B}_{\mathrm{sc}} \end{bmatrix}, \tag{134}$$

where $\hat{B}_{\mathrm{sc}} = I_3$. Note that we do not use knowledge of the wheel inertias J_{W_i}. The negative sign in $\hat{H}_1$ accounts for the negative sign in B_{sc}. As in the thruster case we introduce a proportional saturation on the control input, in this case the angular
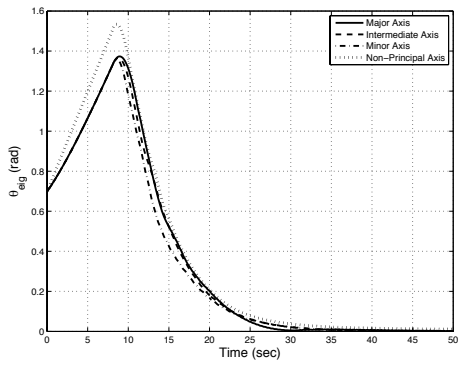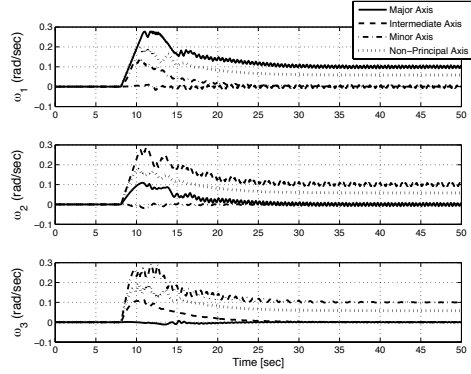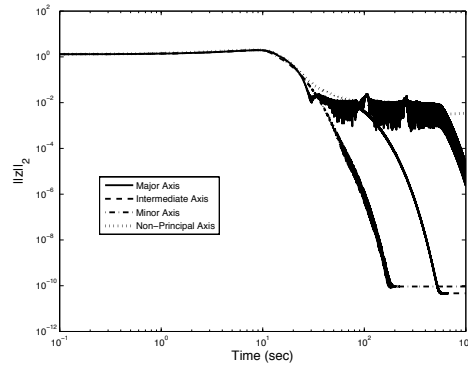
Figure 36. M2S performance for the RCAC control law using thrusters. (a) Eigenaxis attitude error, (b) angular velocity components, and (c) euclidean norm of performance variable. The spacecraft is commanded to spin about each principal body-fixed axis as well as a non-principal axis. The number of previous time steps in the retrospective cost is set to $s = 1$, and the inertia-free Markov parameter $\hat{H}_1$ is given by (120). The saturation level is set at 1 N-m.

acceleration of the wheel.

1. Inertia Variations

For the reaction wheel case we test variations in the spacecraft inertia $J_{\rm sc}$ and the wheel inertias J_{W_i}. First, we start with the centroid inertia J_3 and vary the inertia according to (123). Figure 37 shows the settling time for the M2R maneuver as a function of the inertia parameter α.

In the second approach we use the spacecraft inertia $J_{\rm sc} = J_3$ and let the reaction wheel spin axis inertias $J_{W_i} = \alpha_J$. We vary the reaction wheel inertia parameter $J_{\rm RW}$ and examine the settling time for the M2R maneuver in Figure 38.
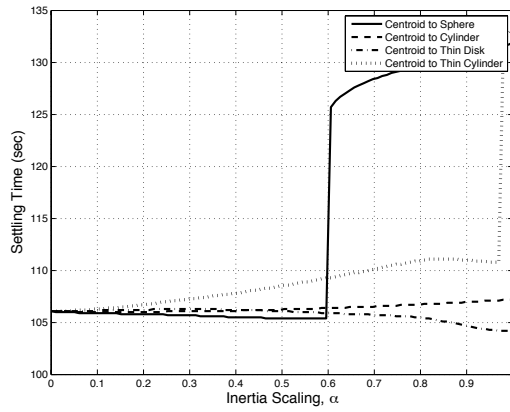
Figure 37. M2R settling time for the RCAC control law using reaction wheels. The inertia J_{sc} starts at the centroid value J_3 and moves toward the sphere J_1, cylinder J_2, thin disk J_4, and thin cylinder J_5 according to (123). The saturation level is set at 0.1 rad/sec^2.
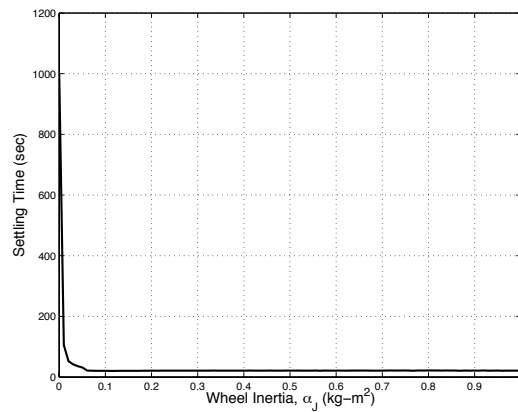
Figure 38. M2R closed-loop performance for the RCAC control law using reaction wheels. The settling time is plotted as a function of the reaction-wheel spin-axis inertia α_J. The saturation level is set at 0.1 rad/sec^2.

D. M2S Maneuvers Using Reaction Wheels

For the M2S maneuver, we again take the spacecraft inertia to be $J_{sc} = J_3$, the reaction wheel inertias $J_{W_i} = 0.1$ kg-m^2 and let the spacecraft be initially at rest so that $R(0) = I$. As in the thruster examples, we test four maneuvers: spins about each of the principal axes and a spin about a non-principal axis.

For the desired attitude, we command an $40°$ eigenaxis rotation about the vector $[1\ 1\ 1]^T$. The desired attitude evolves according to $\dot{R}_d = R_d \omega^\times$. Figure 39 shows the closed-loop response for the M2S maneuver.

(a)

(b)

(c)
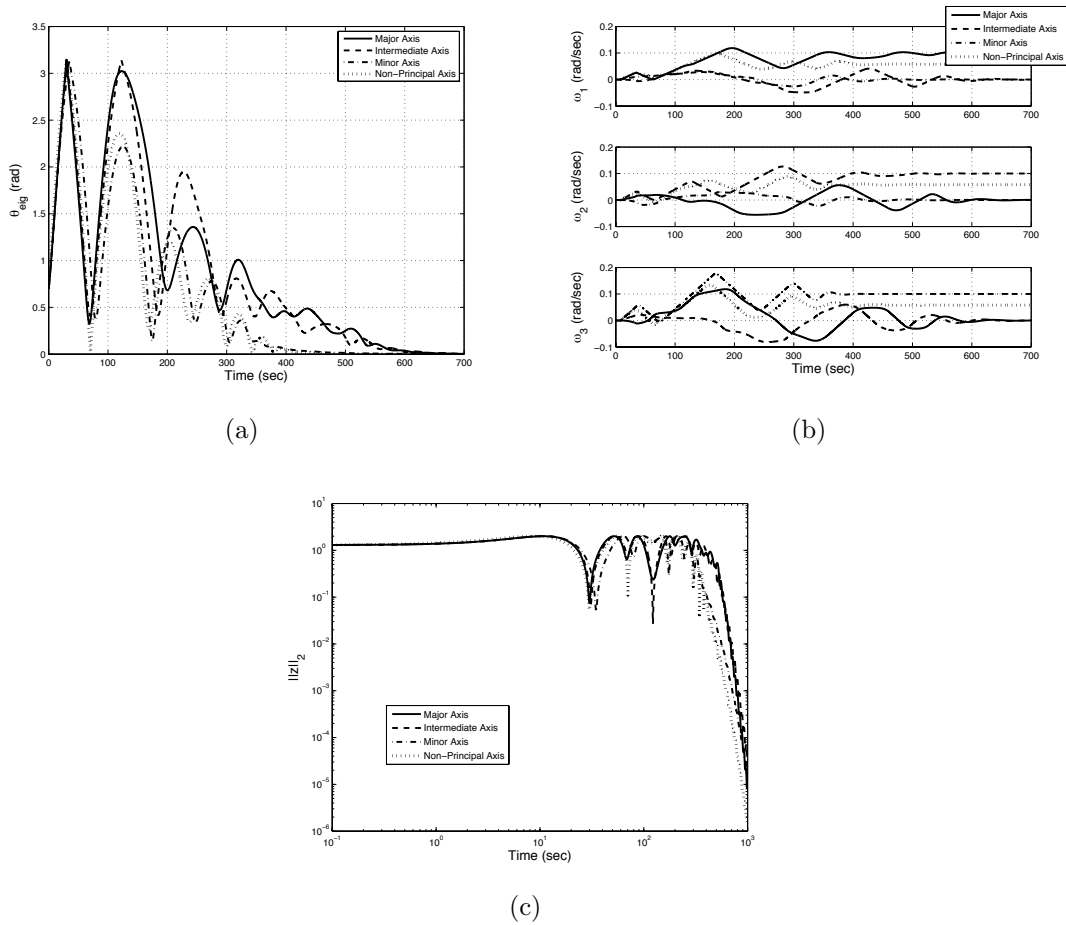
Figure 39. M2S performance for the RCAC control law using reaction wheels. (a) Eigenaxis attitude error, (b) angular velocity components, and (c) euclidean norm of performance variable, The spacecraft is commanded to spin about each principal axis as well as a non-principal axis. The number of previous time steps in the retrospective cost is set to $s = 1$, and the inertia-free Markov parameter $\hat{H}_1$ is given by (134). The saturation level is set at 0.1 rad/sec^2.

X. Future Research

This study has focused on rotation-matrix-based, inertia-free control laws for M2R and M2S maneuvers. To examine the performance of these control laws we considered the effects of possibly unmodeled disturbances, sensor noise, sensor and actuator misalignment, and actuator nonlinearities. Future work will consider additional effects, including time-varying inertia due, for example, to on-orbit deployment of structural components [64]; non-rigid motion due, for example, to structural modes and fuel slosh; multibody spacecraft involving articulated components; time delays in the feedback path that are possibly unknown and time varying; underactuation and undersensing possibly due to failed actuators and sensors; mixed actuation architectures, for example, a combination of magnetic torquers and wheels; alternative control devices, such as devices for atmospheric drag modification; and, finally, the interaction between attitude and orbital dynamics.

References

[1] Stickler, A. and Alfriend, K., "An elementary magnetic attitude control system," *J. Spacecraft and Rockets*, Vol. 13, 1976, pp. 282–287.

[2] Lovera, M. and Astolfi, A., "Global Magnetic Attitude Control of Spacecraft in the Presence of Gravity Gradient," *IEEE Trans. Aerospace Electronic Sys.*, Vol. 42, 2006, pp. 796–805.

[3] Lovera, M. and Astolfi, A., "Spacecraft attitude control using magnetic actuators," *Automatica*, Vol. 40, 2004, pp. 1405–1414.

[4] "Global Magnetic Attitude Control of Inertially Pointing Spacecraft," *AIAA J. Guid. Contr. Dyn.*, Vol. 28, 2005, pp. 1065–1067.

[5] Silani, E. and Lovera, M., "Magnetic Spacecraft Attitude Control: A Survey and Some New Results," *Control Engineering Practice*, Vol. 13, 2005, pp. 357–371.

[6] Junkins, J. L., Akella, M. R., and Robinett, R. D., "Nonlinear Adaptive Control of Spacecraft Maneuvers," *AIAA J. Guid. Contr. Dyn.*, Vol. 20, 1997, pp. 1104–1110.

[7] Egeland, O. and Godhavn, J.-M., "Passivity-Based Adaptive Attitude Control of a Rigid Spacecraft," *IEEE Transactions on Automatic Control*, Vol. 39, 1994, pp. 842–846.

[8] Ahmed, J., Coppola, V. T., and Bernstein, D. S., "Asymptotic Tracking of Spacecraft Attitude Motion with Inertia Identification," *AIAA J. Guid. Contr. Dyn.*, Vol. 21, 1998, pp. 684–691.

[9] Wen, J. T.-Y. and Kreutz-Delgado, K., "The Attitude Control Problem," *IEEE Transactions on Automatic Control*, Vol. 36, 1991, pp. 1148–1162.

[10] Shuster, M. D., "A Survey of Attitude Representations," *Journal of the Astronautical Sciences*, Vol. 41, 1993, pp. 439–517.

[11] Schaub, H. and Junkins, J. L., *Analytical Mechanics of Space Systems*, AIAA, 2003.

[12] Bhat, S. P. and Bernstein, D. S., "A Topological Obstruction to Continuous Global Stabilization of Rotational Motion and the Unwinding Phenomenon," *Sys. Contr. Lett.*, Vol. 39, 2000, pp. 63–70.

[13] Wie, B. and Barba, P. M., "Quaternion Feedback for Spacecraft Large Angle Maneuvers," *AIAA J. Guid. Contr. Dyn.*, Vol. 8, 1985, pp. 360–365.

[14] Joshi, S. M., Kelkar, A. G., and Wen, J. T., "Robust attitude stabilization using nonlinear quaternion feedback," *IEEE Trans. Autom. Contr.*, Vol. 40, 1995, pp. 1148–1161.

[15] Crassidis, J. L., Vadali, S. R., and Markley, F. L., "Optimal Variable-Sructure Control Tracking of Spacecraft Maneuvers," *AIAA J. Guid. Contr. Dyn.*, Vol. 23, 2000, pp. 564–566.

[16] Mayhew, C. G., Sanfelice, R. G., and Teel, A. R., "Quaternion-Based Hybrid Control for Robust Global Attitude Tracking," *IEEE Trans. Autom. Contr.*, Vol. 56, 2011, pp. 2555–2566.

[17] Cortes, J., "Discontinuous Dynamical Systems: A tutorial on solutions, nonsmooth analysis, and stability," *IEEE Contr. Sys. Mag.*, Vol. 28, No. 3, 2008, pp. 36–73.

[18] Chaturvedi, N., Sanyal, A. K., and McClamroch, N. H., "Rigid Body Attitude Control: Using rotation matrices for continuous, singularity-free control laws," *IEEE Contr. Sys. Mag.*, Vol. 31, No. 3, 2011, pp. 30–51.

[19] Koditschek, D. E., "The Application of Total Energy as a Lyapunov Function for Mechanical Control Systems," *Dynamics and Control of Multibody Systems; Proc. AMS-IMS-SIAM Joint Summer Research Conference*, American Mathematical Society, Providence, RI, July 1988, pp. 131–157.

[20] Chaturvedi, N. A., McClamroch, N. H., and Bernstein, D. S., "Asymptotic Smooth Stabilization of the Inverted 3D Pendulum," *IEEE Transactions on Automatic Control*, Vol. 54, 2009, pp. 1204–1215.

[21] Chaturvedi, N. A., McClamroch, N. H., and Bernstein, D. S., "Stabilization of a 3D Axially Symmetric Pendulum," *Automatica*, Vol. 44, 2008, pp. 2258–2265.

[22] Sanyal, A., Fosbury, A., Chaturvedi, N., and Bernstein, D. S., "Inertia-Free Spacecraft Attitude Tracking with Disturbance Rejection and Almost Global Stabilization," *AIAA J. Guid. Contr. Dyn.*, Vol. 32, 2009, pp. 1167–1178.

[23] Mahony, R., Hamel, T., and Pflimlin, J., "Nonlinear complementary filters on the special orthogonal group," *IEEE Trans. Autom. Control*, Vol. 53, 2008, pp. 1203–1218.

[24] Markley, F. L., "Attitude filtering on SO(3)," *J. Astronautical Sciences*, Vol. 54, No. 3–4, 2006, pp. 391–413.

[25] Sanyal, A. K., Lee, T., Leok, M., and McClamroch, N. H., "Global Optimal Attitude Estimation Using Uncertainty Ellipsoids," *Sys. Contr. Lett.*, Vol. 57, 2008, pp. 236–245.

[26] Chaturvedi, N. A., *Global Dynamics and Stabilization of Rigid Body Attitude Systems*, Ph.D. thesis, University of Michigan, Ann Arbor, MI, 2007.

[27] Weiss, A., Yang, X., Kolmanovsky, I., and Bernstein, D. S., "Inertia-Free Spacecraft Attitude Control with Reaction-Wheel Actuation," *Proc. AIAA Guid. Nav. Contr. Conf.*, Toronto, August 2010, AIAA-2010-8297-163.

[28] Agarwal, K., Weiss, A., Kolmanovsky, I., and Bernstein, D. S., "Inertia-Free Spacecraft Attitude Control with Control-Moment-Gyro Actuation," *Proc. AIAA Guid. Nav. Contr. Conf.*, Minneapolis, MN, August 2012, AIAA-2012-5003-282.

[29] Cruz, G., Yang, X., Weiss, A., Kolmanovsky, I., and Bernstein, D. S., "Torque-saturated, Inertia-free Spacecraft Attitude Control," *Proc. AIAA Guid. Nav. Contr. Conf.*, Portland, OR, August 2011, AIAA-2011-6507.

[30] Wie, B., *Space Vehicle Dynamics and Control*, AIAA, 2nd ed., 2008.

[31] Hoagg, J. B., Santillo, M. A., and Bernstein, D. S., "Discrete-time Adaptive Command Following and Disturbance Rejection with Unknown Exogenous Dynamics," *IEEE Trans. Autom. Contr.*, Vol. 53, 2008, pp. 912–928.

[32] Hoagg, J. B. and Bernstein, D. S., "Retrospective Cost Adaptive Control for Nonminimum-Phase Discrete-Time Systems Part 1: The Ideal Controller and Error System, Part 2: The Adaptive Controller and Stability Analysis," *Proc. Conf. Dec. Contr.*, Atlanta, GA, December 2010, pp. 893–904.

[33] Hoagg, J. B. and Bernstein, D. S., "Retrospective Cost Model Reference Adaptive Control for Nonminimum-Phase Discrete-Time Systems, Part 1: The Adaptive Controller; Part 2: Stability Analysis," *Proc. Amer. Contr. Conf.*, San Francisco, CA, June 2011, pp. 2927–2938.

[34] Santillo, M. A. and Bernstein, D. S., "Adaptive Control Based on Retrospective Cost Optimization," *AIAA J. Guid. Contr. Dyn.*, Vol. 33, 2010, pp. 289–304.

[35] D'Amato, A. M., Sumer, E. D., and Bernstein, D. S., "Frequency-Domain Stability Analysis of Retrospective-Cost Adaptive Control for Systems with Unknown Nonminimum-Phase Zeros," *Proc. Conf. Dec. Contr.*, Orlando, FL, December 2011, pp. 1098–1103.

[36] Sumer, E. D., D'Amato, A. M., Morozov, A. M., Hoagg, J. B., and Bernstein, D. S., "Robustness of Retrospective Cost Adaptive Control to Markov-Parameter Uncertainty," *Proc. Conf. Dec. Contr.*, Orlando, FL, December 2011, pp. 6085–6090.

[37] Morozov, A. V., Hoagg, J. B., and Bernstein, D. S., "Retrospective Adaptive Control of a Planar Multilink Arm with Nonminimum-Phase Zeros," *Proc. Conf. Dec. Contr.*, Atlanta, GA, December 2010, pp. 3706–3711.

[38] Yan, J., D'Amato, A. M., Sumer, D., Hoagg, J. B., and Bernstein, D. S., "Adaptive Control of Uncertain Hammerstein Systems Using Auxiliary Nonlinearities," *Proc. Conf. Dec. Contr.*, Maui, HI, December 2012.

[39] Cruz, G., D'Amato, A. M., and Bernstein, D. S., "Retrospective Cost Adaptive Control of Spacecraft Attitude," *Proc. AIAA Guid. Nav. Contr. Conf.*, Minneapolis, MN, August 2012.

[40] Cruz, G. and Bernstein, D. S., "Adaptive Spacecraft Attitude Control with Reaction-Wheel Actuation," *Proc. Conf. Dec. Contr.*, Washington, DC, June 2013, submitted.

[41] Bhat, S., "Controllability of Nonlinear Time-varying Systems: Applications to Spacecraft Attitude Control Using Magnetic Actuation," *IEEE Trans. Autom. Control*, Vol. 50, 2005, pp. 1725–1735.

[42] Cullity, B. D. and Graham, C. D., *Introduction to Magnetic Materials*, John Wiley & Sons, 2nd ed., 2008.

[43] Lee, J., Ng, A., and Jobanputra, R., "On Determining Dipole Moments of a Magnetic Torquer Rod - Experiments and Discussion," *J. Aeronautique et Spatial De Canada*, Vol. 48, 2002, pp. 61–67.

[44] Finlay, C. C. and et al, "International Geomagnetic Reference Field: the eleventh generation," *Geophysical Journal International*, Vol. 183, No. 3, 2010, pp. 1216–1230.

[45] Lowes, F. J., "The International Geomagnetic Reference Field: A 'Health' Warning," `http://www.ngdc.noaa.gov/IAGA/vmod/igrfhw.html`, January 2011.

[46] Weiss, A., Kolmanovsky, I., and Bernstein, D. S., "Forward-Integration Riccati-Based Feedback Control of Magnetically Actuated Spacecraft," *Proc. AIAA Guid. Nav. Contr. Conf.*, Minneapolis, MN, August 2012, AIAA-2012-5042-137.

[47] Lovera, M. and Astolfi, A., "Global Magnetic Attitude Control of Spacecraft in the Presence of Gravity Gradient," *Transactions on Aerospace and Electronic Systems*, Vol. 42, No. 3, 2006, pp. 796–805.

[48] Leve, F., Boyarko, G. A., and Fitz-Coy, N. G., "Precise Torque Mapping for Pico-Satellite Single-Gimbal Control Moment Gyroscopes," *Advances in the Astronautical Sciences, Vol. 137, Univelt, Inc., San Diego, CA, 2010, also AAS/AIAA Paper AAS 10-095, 33rd Annual AAS Guidance and Control Conference*, Breckenridge, CO, February 2010.

[49] Meng, T. and Matunaga, S., "Modified Singular-Direction Avoidance Steering for Control Moment Gyros," *Journal of Guidance, Control, and Dynamics*, Vol. 34, No. 6, 2011, pp. 1915–1919.

[50] Pechev, A., "Feedback-Based Steering Law for Control Moment Gyros," *Journal of Guidance, Control, and Dynamics*, Vol. 30, No. 3, 2007, pp. 848–855.

[51] Wie, B., "Singularity Analysis and Visualization for Single-Gimbal Control Moment Gyro Systems," *Journal of Guidance, Control, and Dynamics*, Vol. 27, No. 2, 2004, pp. 271–282.

[52] Kurokawa, H., "A Geometry Study of Single Gimbal Control Moment Gyros–Singularity Problem and Steering Law," *TR 175*, Mechanical Engineering Lab., Tsukuba, Ibaraki, Japan, 1998.

[53] Takada, K., Kojima, H., and Matsuda, N., "Control Moment Gyro Singularity-Avoidance Steering Control Based on Singular-Surface Cost Function," *Journal of Guidance, Control, and Dynamics*, Vol. 33, No. 5, 2010, pp. 1442–1450.

[54] Wie, B., "Singularity Robust Steering Logic for Redundant Single-Gimbal Control Moment Gyros," *Journal of Guidance, Control, and Dynamics*, Vol. 24, No. 5, 2001, pp. 865–872.

[55] Paradiso, J. A., "Global Steering of Single Gimbaled Control Moment Gyroscopes using a Directed Search," *Journal of Guidance, Control, and Dynamics*, Vol. 15, No. 5, 1992, pp. 1236–1244.

[56] Nakamura, Y. and Hanafusa, H., "Inverse Kinematic Solutions with Singularity Robustness for Robot Manipulator Control," *Journal of Dynamic Systems, Measurement, and Control*, Vol. 108, Sept. 1986, pp. 163–171.

[57] Bedrossian, N. S., *Steering Law Design for Redundant Single Gimbal Control Moment Gyro Systems*, M.s. thesis, Massachusetts Inst. of Technology, Cambridge, MA, Aug. 1987.

[58] Hoagg, J. B., Santillo, M. A., and Bernstein, D. S., "Internal Model Control in the Shift and Delta Domains," *IEEE Trans. Autom. Contr.*, Vol. 53, 2008, pp. 1066–1072.

[59] Praly, L., Hung, S. T., and Rhode, D. S., "Towards a Direct Adaptive Scheme for a Discrete-Time Control of a Minimum Phase Continuous-Time System," *Proc. Conf. Dec. Contr.*, Fort Lauderdale, FL, December 1989, pp. 1188–1191.

[60] Venugopal, R. and Bernstein, D. S., "Adaptive Disturbance Rejection Using AR-MARKOV System Representations," *IEEE Trans. Contr. Sys. Tech.*, Vol. 8, 2000, pp. 257–269.

[61] D'Amato, A. M., Sumer, E. D., and Bernstein, D. S., "Retrospective Cost Adaptive Control for Systems with Unknown Nonminimum-Phase Zeros," *AIAA Guid. Nav. Contr. Conf.*, Portland, OR, August 2011, AIAA-2011-6203.

[62] D'Amato, A. M., Sumer, E. D., Mitchell, K. S., Morozov, A. V., Hoagg, J. B., and Bernstein, D. S., "Adaptive Output Feedback Control of the NASA GTM Model with Unknown Nonminimum-Phase Zeros," *AIAA Guid. Nav. Contr. Conf.*, Portland, OR, August 2011, AIAA-2011-6204.

[63] Fledderjohn, M. S., Holzel, M. S., Palanthandalam-Madapusi, H., Fuentes, R. J., and Bernstein, D. S., "A Comparison of Least Squares Algorithms for Estimating Markov Parameters," *Proc. Amer. Contr. Conf.*, Baltimore, MD, June 2010, pp. 3735–3740.

[64] Weiss, A., Kolmanovsky, I., and Bernstein, D. S., "Inertia-Free Attitude Control of Spacecraft with Unknown Time-Varying Mass Distribution," *Proc. 62nd IAC*, Cape Town, South Africa, October 2011, IAC-11-C1.5.9.